Inorganic Chemistry
Cite This: Inorg. Chem. XXXX, XXX, XXX−XXX
Article
pubs.acs.org/IC

# α-Diimines as Versatile, Derivatizable Ligands in Ruthenium(II) p-Cymene Anticancer Complexes

Lorenzo Biancalana,[†] Lucinda K. Batchelor,[‡] Tiziana Funaioli,[†] Stefano Zacchini,[§] Marco Bortoluzzi,[∥] Guido Pampaloni,[†] Paul J. Dyson,[‡] and Fabio Marchetti*[,†]

[†]Dipartimento di Chimica e Chimica Industriale, Università di Pisa, Via G. Moruzzi 13, I-56124 Pisa, Italy
[‡]Institut des Sciences et Ingénierie Chimiques, Ecole Polytechnique Fédérale de Lausanne, CH-1015 Lausanne, Switzerland
[§]Dipartimento di Chimica Industriale "Toso Montanari", Università di Bologna, Viale Risorgimento 4, I-40136 Bologna, Italy
[∥]Dipartimento di Scienze Molecolari e Nanosistemi, Università Ca' Foscari Venezia, Via Torino 155, I-30170 Mestre, Venice, Italy

Supporting Information

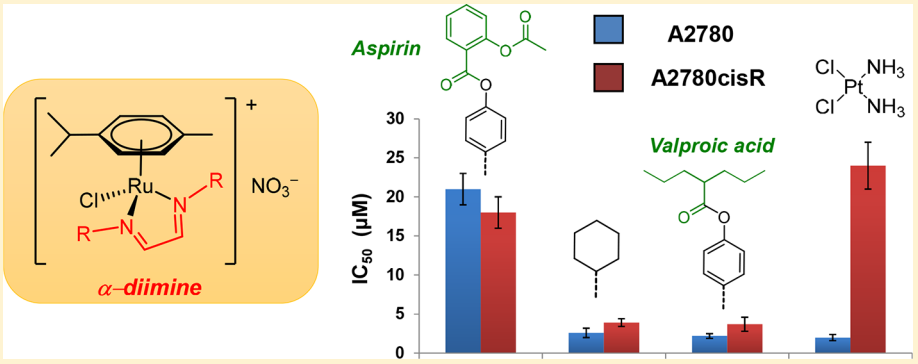


**ABSTRACT:** α-Diimines are among the most robust and versatile ligands available in synthetic coordination chemistry, possessing finely tunable steric and electronic properties. A series of novel cationic ruthenium(II) *p*-cymene complexes bearing simple α-diimine ligands, $[(\eta^6\text{-}p\text{-cymene})RuCl\{\kappa^2N\text{-}(HCNR)_2\}]NO_3$ (R = Cy, [**1**]$NO_3$; R = 4-$C_6H_{10}OH$, [**2**]$NO_3$; R = 4-$C_6H_4OH$, [**3**]$NO_3$), were prepared in near-quantitative yields as their nitrate salts. [**2**]$NO_3$ displays high water solubility. The potential of the α-diimine ligand in [**3**]$NO_3$ as a carrier of bioactive molecules was investigated via esterification reactions with the hydroxyl groups. Thus, the double-functionalized derivatives $[(\eta^6\text{-}p\text{-cymene})RuCl\{\kappa^2N\text{-}(HCN(4\text{-}C_6H_4OCO\text{-}R))_2\}]NO_3$ (R = aspirinate, [**5**]$NO_3$; valproate, [**6**]$NO_3$) and also [**4**]Cl (R = Me) were obtained in good-to-high yields. UV−vis and multinuclear NMR spectroscopy and cyclic voltammetric studies in aqueous solution revealed only minor ruthenium chloride hydrolytic cleavage, biologically accessible reduction potentials, and pH-dependent behavior of [**3**]$NO_3$. Density functional theory analysis was performed in order to compare the Ru−Cl bond strength in $[\mathbf{1}]^+$ with the analogous ethylenediamine complex, showing that the higher stability observed in the former is related to the electron-withdrawing properties of the α-diimine ligand. In vitro cytotoxicity studies were performed against tumorigenic (A2780 and A2780cisR) and nontumorigenic (HEK-293) cell lines, with the complexes bearing simple α-diimine ligands ranging from inactive to $IC_{50}$ values in the low micromolar range. The complexes functionalized with bioactive components, i.e., [**5**]$NO_3$ and [**6**]$NO_3$, exhibited a marked increase in the cytotoxicity with respect to the precursor [**3**]$NO_3$.

## INTRODUCTION

The introduction of cisplatin into clinics over 40 years ago generated widespread interest in platinum complexes as viable anticancer drugs. However, despite the efficacy of cisplatin and other platinum complexes toward many types of cancers, problems are associated with their use including severe side effects and the progressive acquisition of drug resistance. Consequently, considerable efforts have been invested in the development of alternative metal-based anticancer drugs that overcome the limitations of platinum chemotherapics.[1] Ruthenium compounds are regarded as promising candidates for the next generation of metal anticancer drugs.[1b−e,2] Two ruthenium(III) compounds, i.e., [imidazoleH][*trans*-Ru(κ*N*-imidazole)(κ*S*-DMSO)$Cl_4$] (NAMI-A) and [indazoleH][*trans*-Ru(κ*N*-indazole)$_2Cl_4$] (KP1019; Figure 1), and a sodium salt, Na[*trans*-Ru(κ*N*-indazole)$_2Cl_4$] (NKP-1339/IT139), have entered phase I/II clinical trials.[3] These ruthenium(III) species are believed to act as prodrugs and are reduced to their more active ruthenium(II) counterparts in the hypoxic tumor environment.[4] Bypassing the prodrug characteristics, ruthenium(II) complexes, especially those based on the

Received: April 2, 2018




DOI: 10.1021/acs.inorgchem.8b00882
Inorg. Chem. XXXX, XXX, XXX−XXX

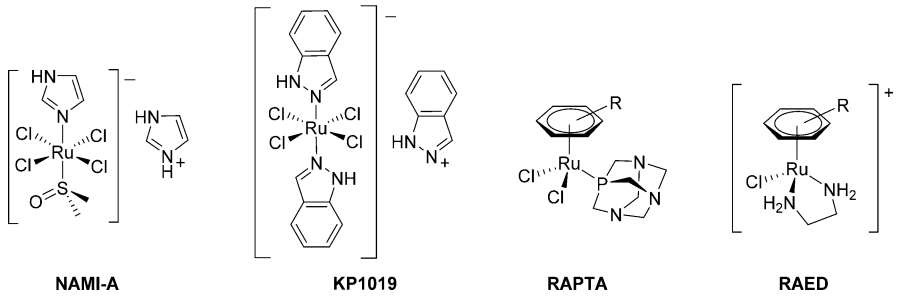


**Figure 1.** Relevant ruthenium compounds exhibiting anticancer activity.

**Scheme 1. Structures and General Synthetic Procedure for $\alpha$-Diimine Ligands L1−L3**

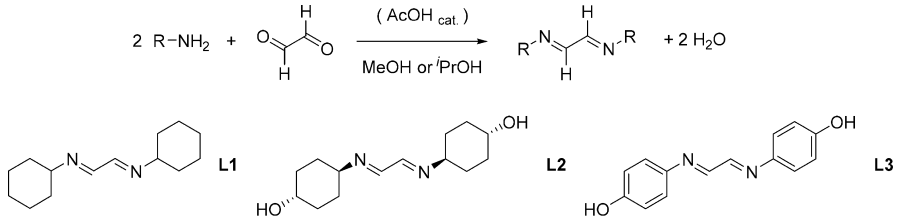


**Scheme 2. Synthesis of Ruthenium(II) *p*-Cymene Complexes with $\alpha$-Diimine Ligands, [1−3]$NO_3$**

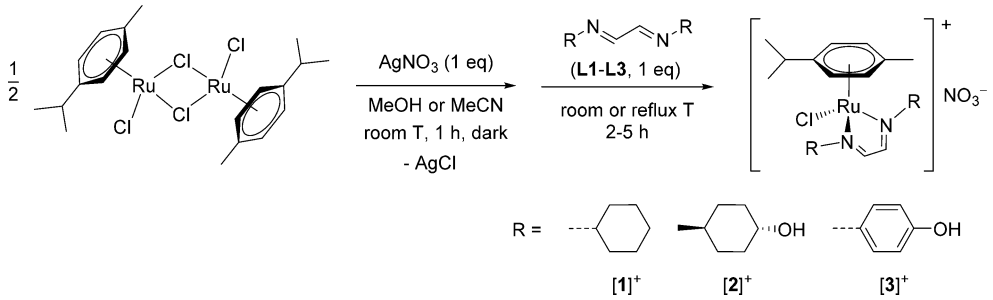


ruthenium(II) $\eta^6$-arene scaffold, have attracted considerable attention.[5] In particular, the RAPTA series, bearing a 1,3,5-triaza-7-phosphatricyclo[3.3.1.1]decane (PTA) ligand,[6] and RAED complexes, possessing an ethylene-1,2-diamine (en) ligand,[7] are considered to be prominent species exhibiting significant antitumor activity in vivo (Figure 1).

A wide range of ruthenium $\eta^6$-arene complexes with modified ligands were developed with the aim of improving their anticancer properties. In the case of the RAED complexes, the en ligand has been replaced with substituted diamines[8] and many N,N-chelating ligands,[9] and the resulting compounds were tested against various cancer cell lines.

$\alpha$-Diimines (also called 1,4-diaza-1,3-dienes) are among the most robust and versatile ligands available in synthetic coordination chemistry and possess finely tunable steric and electronic properties.[10] Although some ruthenium $\eta^6$-arene complexes with $\alpha$-diimine ligands, i.e., (R)N═C(R′)C(R′)═N(R) (R = alkyl or aryl; R′ = H and Me) were reported, they did not undergo biological evaluation.[11]

A promising strategy used to optimize the anticancer activity of metal complexes involves the inclusion of bioactive organic fragments. This approach is designed to enhance the interaction of the resulting compounds with specific targets overexpressed or uniquely expressed in cancer cells.[12] Thus, a range of organic groups with known biological functions have been directly coordinated to the ruthenium(II) center,[13] tethered to the arene,[14] or introduced via nitrogen and phosphorus ligands.[15]

Herein, we describe the synthesis and characterization of stable, significantly water ($H_2O$)-soluble ruthenium(II) *p*-cymene-$\alpha$-diimine complexes, demonstrating that a specific $\alpha$-diimine ligand with phenolic substituents undergoes clean functionalization with bioactive carboxylic acids. The cytotoxicity of the compounds was evaluated and is discussed with respect to the spectroscopic and electrochemical properties of the complexes in an aqueous solution.

## RESULTS AND DISCUSSION

**Synthesis and Characterization of the $\alpha$-Diimine Ligands and Their Ruthenium(II) *p*-Cymene Complexes.** $\alpha$-Diimine ligands, of the general formula (R)N═CHCH═N(R) (R = $C_6H_{11}$ = Cy, **L1**;[16] R = 4-$C_6H_{10}$OH, **L2**; R = 4-$C_6H_4$OH, **L3**[17]), were prepared via the acid-catalyzed condensation of glyoxal with the appropriate primary amine in alcohols (Scheme 1). The synthesis of the unprecedented **L2** (47% yield) and that of **L3** (82% yield) were optimized with varying solvent and temperature. The salient IR, NMR, and UV−vis data of **L1**−**L3** are compiled in Table S1.

The preparation of the ruthenium $\alpha$-diimine compounds [($\eta^6$-*p*-cymene)RuCl{$\kappa^2$*N*-(HCNR)$_2$}]$NO_3$ (R = Cy, [**1**]$NO_3$; R = 4-$C_6H_{10}$OH, [**2**]$NO_3$; R = 4-$C_6H_4$OH, [**3**]$NO_3$) was achieved via the reaction of the dimer [(*p*-cymene)$RuCl_2$]$_2$ with $AgNO_3$, followed by the addition of the $\alpha$-diimine (ruthnium/silver/$\alpha$-diimine ratio 1:1:1; Scheme 2). At variance with the literature,[10] $AgNO_3$ was selected as an unusual but


DOI: 10.1021/acs.inorgchem.8b00882
Inorg. Chem. XXXX, XXX, XXX−XXX

convenient chloride abstractor because it does not require inert and anhydrous conditions. The choice of solvent [acetonitrile (MeCN) or methanol (MeOH)] and reaction temperature proved crucial to achieving full conversion and high selectivity. The products were isolated as air-stable orange ([**1**,**2**]$NO_3$) or dark-red/brown ([**3**]$NO_3$) solids in high yields (93−98%).

Complexes [**1**−**3**]$NO_3$ are soluble in $H_2O$ (a detailed discussion of their solubility and stability in an aqueous medium is given below). Compound [**1**]$NO_3$ is also soluble in common organic solvents excluding diethyl ether ($Et_2O$) and hydrocarbons, whereas [**2**,**3**]$NO_3$, bearing hydroxyl groups on the N-substituents, are insoluble in chlorinated solvents but soluble in alcohols and dimethyl sulfoxide (DMSO).

The products were fully characterized using analytical techniques (CHN analysis, mass spectrometry, and conductivity) and NMR, IR, and UV−vis spectroscopy (selected data are compiled in Table S1). The $^1$H and $^{13}$C NMR spectra of [**1**]$NO_3$, recorded in deuterated chloroform ($CDCl_3$), and [**2**,**3**]$NO_3$, in $CD_3OD$ or DMSO-$d_6$, contain a single set of resonances for the *p*-cymene and $\alpha$-diimine ligands. A singlet, corresponding to the two imine protons of the coordinated ligand, was observed at 8.3−8.4 ppm, i.e., slightly deshielded ($\Delta\delta_H \leq 0.4$ ppm) with respect to uncoordinated **L1**−**L3**. The imine carbon experiences a more significant downfield shift ($\Delta\delta_C = 4-9$ ppm) with a resonance around 165 ppm in the $^{13}$C NMR spectra of [**1**−**3**]$NO_3$, compared to 156.0−160.2 ppm for the free $\alpha$-diimine. Signals relating to the hydroxyl group protons of [**2**]$^+$ and [**3**]$^+$ are observed in the $^1$H NMR spectra at 4.7 and 10.4 ppm in DMSO-$d_6$, respectively, and remain at a value comparable to that of the corresponding ligands **L2** and **L3**. In DMSO-$d_6$, the $^1$H resonances of [**3**]$NO_3$ are broad, and negligible changes are observed with increasing temperature from 25 to 60 °C. This suggests that a strong $NO_3^-$/[**3**]$^+$ interaction (and related association phenomena[11a,b]) takes place in DMSO-$d_6$ and presumably involves hydrogen bonding with the phenolic groups. Well-resolved $^1$H NMR spectra were recorded for [**3**]$NO_3$ in $CD_3OD$ and for [**2**]$NO_3$ in both DMSO-$d_6$ and $CD_3OD$ solutions, which indicated that the ions are well solvated and separated.

The UV−vis spectra of [**1**−**3**]$NO_3$ in $CH_2Cl_2$ or MeOH feature metal-to-ligand charge-transfer (MLCT) bands around 270−280 and 420−450 nm.[10c] Increased band intensity ($\varepsilon$) and an additional absorption at ca. 550 nm were observed for [**3**]$NO_3$, which contains an extended $\pi$ system in the $\alpha$-diimine ligand.

The solid-state IR spectra of [**1**−**3**]$NO_3$ show strong absorptions due to the $[NO_3]^-$ ion (ca. 1320 cm$^{-1}$) and medium/weak C═N stretching vibrations in the region 1530−1630 cm$^{-1}$. The relative intensity of this C═N absorption is lower in the complexes compared to the respective uncoordinated $\alpha$-diimines, and a considerable decrease in the wavenumber (ca. −85 cm$^{-1}$) is observed upon coordination of **L1** and **L2**.[18]

The solid-state structure of [**1**]$NO_3$ was determined by single-crystal X-ray diffraction (Figure 2), and relevant parameters are presented in Table 1. The cation [**1**]$^+$ possesses the expected three-legged piano-stool geometry typical of other ruthenium(II) arene compounds,[19] and the bonding parameters around the ruthenium(II) center are similar to those reported for related [(*p*-cymene)RuCl($\alpha$-diimine)]$^+$ structures.[11a] Moreover, C−C and C−N distances within the main skeleton of the **L1** ligand are comparable to those previously observed in $RuCl_2$(**L1**)$_2$.[20]

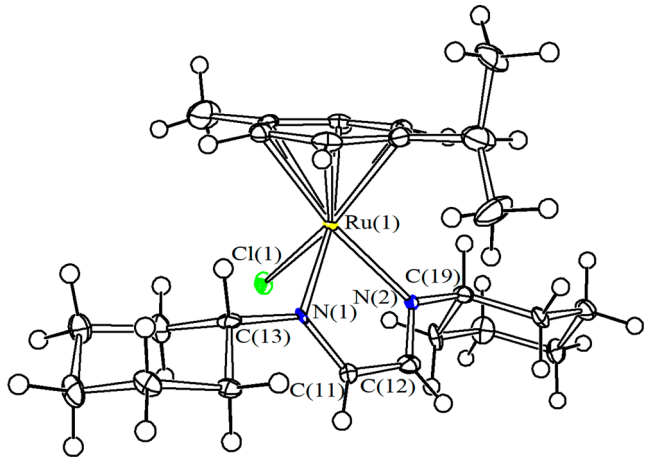


**Figure 2.** Molecular structure of [**1**$^+$] within [**1**]$NO_3$. Displacement ellipsoids are at the 50% probability level.

**Derivatization of the Complexes with Bioactive Groups.** In principle, the OH groups belonging to the $\alpha$-diimines **L2** and **L3** could be exploited for functionalization; in particular, esterification reactions may represent a strategy to incorporate bioactive molecules featuring −$CO_2H$ groups within (*p*-cymene)Ru$^{II}$ complexes via $\alpha$-diimine linkers.

Our first attempts, using various synthetic protocols,[21] to perform the esterification of **L2** and **L3** with different carboxylic acids afforded mixtures of products, and the $\alpha$-diimine moiety did not tolerate the conditions used. This is in alignment with literature reports, indicating that functionalization of the arene ring in *N*-aryl-$\alpha$-diimine systems is usually achieved prior to generation of the imine skeleton.[22] Upon further investigation, we noticed that two esterification reactions of **L3**, coordinated in transition-metal complexes, were previously described.[23] Therefore, we focused on the direct esterification of **L2** and **L3** coordinated to the ($\eta^6$-*p*-cymene)Ru frame in the corresponding complexes [**2**,**3**]$NO_3$.

After several attempts, we found that the addition of an excess of acetyl chloride, as a model reactant, to a refluxing trichloromethane ($CHCl_3$) solution of [**3**]$NO_3$ treated with 1,5-diazabicyclo[5.4.0]undec-7-ene (DBU) resulted in the formation of the diester [**4**]Cl, which was isolated in 68% yield (Scheme 3a). On the other hand, [**2**]$NO_3$ was largely unreactive.

Then, aspirin and valproic acid were selected as viable candidates to functionalize [**3**]$NO_3$. These bioactive molecules contain carboxylic acid groups and are known to possess anticancer properties.[24,25] It was previously demonstrated that the incorporation of aspirin and valproic acid into metal complexes, including (*p*-cymene)Ru$^{II}$ complexes,[15c] can provide a synergism resulting in enhanced cytotoxicity.[26,27]

Because the conditions employed for the synthesis of [**4**]Cl were not suitable to aspirin and valproic acid, *N*-[3-(dimethylamino)propyl]-*N*′-ethylcarbodiimide hydrochloride (EDCI·HCl) and 4-(dimethylamino)pyridine (DMAP) were used as the coupling agent and base catalyst, respectively (Steglich protocol[28]). An excess of the bioactive component was reacted with [**3**]$NO_3$ to yield the bis-functionalized complexes [**5**]$NO_3$ and [**6**]$NO_3$ in 92 and 69% yield, respectively (Scheme 3b). This synthetic route overcomes two common problems usually experienced in this chemistry, i.e., harsh conditions intolerable to the $\alpha$-diimine backbone and


DOI: 10.1021/acs.inorgchem.8b00882
*Inorg. Chem.* XXXX, XXX, XXX−XXX

**Table 1. Selected Bond Distances (Å) and Angles (deg) for $[1]^+$**

| | | | |
|---|---|---|---|
| Ru(1)−($\eta^6$-*p*-cymene)$_{av}$ | 2.20(2) | Ru(1)−Cl(1) | 2.384(2) |
| Ru(1)−N(1) | 2.080(6) | Ru(1)−N(2) | 2.071(6) |
| N(1)−C(11) | 1.279(10) | N(2)−C(12) | 1.269(10) |
| N(1)−C(13) | 1.484(10) | N(2)−C(19) | 1.491(10) |
| C(11)−C(12) | 1.436(11) | | |
| | | | |
| N(1)−Ru(1)−N(2) | 76.5(2) | Ru(1)−N(1)−C(11) | 114.9(5) |
| N(1)−C(11)−C(12) | 116.4(7) | C(11)−C(12)−N(2) | 116.4(7) |
| C(12)−N(2)−Ru(1) | 115.7(5) | | |

**Scheme 3. Esterification of $[3]NO_3$: (a) Preparation of [4]Cl with DBU/MeCOCl and (b) EDCI/DMAP-Mediated Reaction with Aspirin (asp-$CO_2H$) and Valproic Acid (vp-$CO_2H$), Affording Compounds $[5,6]NO_3$**

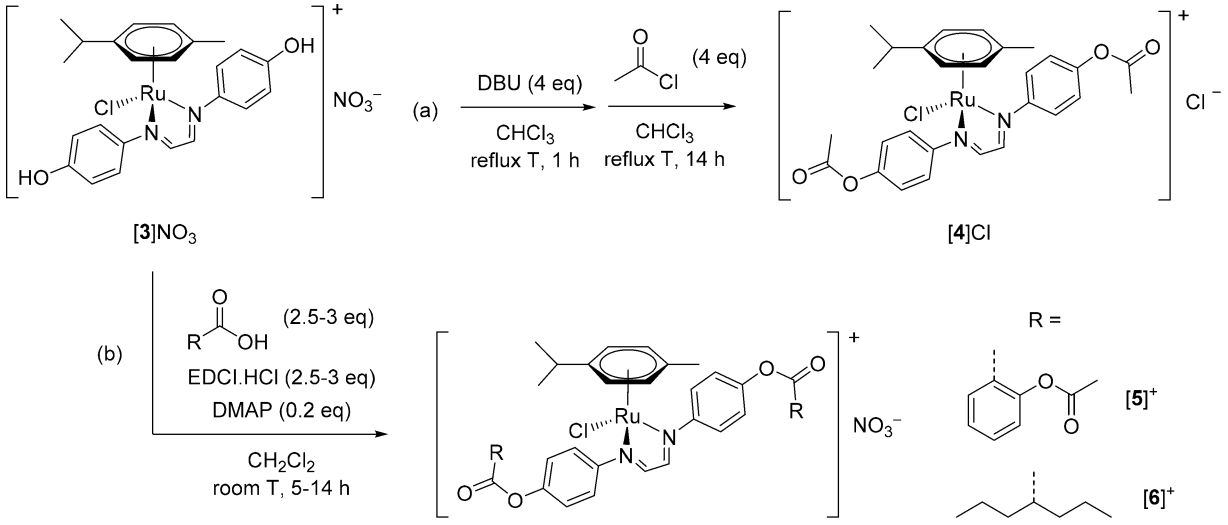


the need to protect the ruthenium center during the peripheral esterification reaction.[6c,15c]

It is noteworthy that two bioactive fragments are associated here with a single ruthenium center; recently, the introduction of two bioactive compounds to a single ruthenium or osmium complex via (bi)pyridine ligands resulted in a significant cytotoxic effect.[15a,29]

Compounds [**4**−**6**]X (X = Cl and $NO_3$) are air-stable dark-red/brown solids that possess good solubility in chlorinated solvents, acetone, and DMSO but have low solubility in MeOH and $H_2O$. The lack of $H_2O$ solubility correlates with the substantial increase in the hydrophobicity of the cation upon going from $[3]^+$ to $[4-6]^+$. The NMR spectroscopic data ($CD_3OD$ solution;[30] Table S1) related to the imine CH units show a small deshielding with respect to the precursor $[3]NO_3$ ($\Delta\delta_H$ = +0.2 ppm; $\Delta\delta_C$ = +3.5 ppm). Conversely, the $^{13}C$ NMR resonance of the carbonyl carbon undergoes a marked upfield shift following the introduction of bioactive molecules relative to the ruthenium(II) $\alpha$-diiminodiester ($\Delta\delta_C \approx -6-7$ ppm). The IR spectra of [**4**−**6**]X (X = Cl and $NO_3$) display a strong absorption in the 1750−1760 $cm^{-1}$ region due to the $\nu$(C═O) stretching of the newly formed ester moiety as well as a medium-weak absorption around 1600 $cm^{-1}$ due to the $\nu$(C═N) stretching.

The presence of chloride or nitrate counterions in [**4**−**6**]X was ascertained using an $X^-/[BF_4]^-$ metathesis assay (see the Supporting Information, SI), IR spectroscopy (the presence or absence of intense $[NO_3]^-$ absorptions around 1335 $cm^{-1}$), and $^{14}N$ NMR spectroscopy. Broad resonances are generally observed in $^{14}N$ NMR spectra because of the quadrupolar nature of the nucleus, with the exception of highly symmetric species such as $[NH_4]^+$ or $[NO_3]^-$.[31] For instance, $NaNO_3$ in a $D_2O$ or $CD_3OD$ solution displayed narrow $^{14}N$ NMR signals at −5.0 or −2.7 ppm, respectively (see the Experimental Section). Consistent with this observation, a signal around −3 ppm was present in the $^{14}N$ NMR spectra of $[5,6]NO_3$ in MeOH, whereas no signal was observed in the spectrum of [**4**]Cl.

**Solubility, Stability, and Speciation of the Complexes in an Aqueous Solution.** Compounds $[1-3]NO_3$ readily dissolve in $H_2O$, affording yellow/red solutions, and the $^1H$ NMR and UV−vis spectra recorded in $D_2O$ resembled those recorded in organic solvents. The solubility of $[1-3]NO_3$ was evaluated in saturated $D_2O$ solutions at 21 °C using $^1H$ NMR spectroscopy with dimethyl sulfone ($Me_2SO_2$), employed as an internal standard.[32] The solubility is $5.6 \times 10^{-3}$ M for $[3]NO_3$ and $1.0 \times 10^{-2}$ M for $[1]NO_3$, reaching 0.1 M for $[2]NO_3$ (Table 2). Considering that $\alpha$-diimines **L1**−**L3** are insoluble in $H_2O$, it appears that the $H_2O$ solubility of $[1-3]NO_3$ is most likely favored by the $[NO_3]^-$ anion rather than a hydrophilic ligand. Conversely, the $H_2O$ solubility of [($\eta^6$-*p*-cymene)-$RuCl_2$(PTA)] (RAPTA-C) and [($\eta^6$-*p*-cymene)RuCl-($NH_2CH_2CH_2NH_2$)]$^+$ (RAED-C) complexes is achieved by the coordination of a $H_2O$-soluble ligand (Figure 1).

The solutions of $[1-3]NO_3$ were then maintained at 37 °C for 72 h, the temperature under which the cell studies were performed, and monitored by $^1H$ and $^{35}Cl$ NMR, UV−vis, and conductivity measurements. Because of limited solubility in $H_2O$, evaluation of the $H_2O$ stability of [**4**−**6**]X (X = Cl and $NO_3$) had to be carried out in DMSO/$H_2O$ (9:1) mixtures. In general, the complexes were stable, with 80−99% of the


DOI: 10.1021/acs.inorgchem.8b00882
Inorg. Chem. XXXX, XXX, XXX−XXX

**Table 2. Solubility of $[1-3]NO_3$ in $D_2O$ and the Fraction of $[1-6]X$ (X = $NO_3$ and Cl) after 72 h at 37 °C in $D_2O$ or DMSO-$d_6$/$D_2O$ (9:1, v/v) Solutions**[a]

| compound | solvent | solubility (21 °C)/mol·L$^{-1}$ | % complex remaining (72 h, 37 °C) |
|---|---|---|---|
| $[1]NO_3$ | $H_2O$ | $1.0 \times 10^{-2}$ | 91 |
| $[2]NO_3$ | $H_2O$ | $1.0 \times 10^{-1}$ | 97 |
| $[3]NO_3$ | $H_2O$ | $5.6 \times 10^{-3}$ | 99 |
| 4[Cl] | 9:1 DMSO/$H_2O$ | | 81 |
| $[5]NO_3$ | 9:1 DMSO/$H_2O$ | | 86 |
| $[6]NO_3$ | 9:1 DMSO/$H_2O$ | | 80 |

[a]All values are based on $^1$H NMR spectroscopy ($Me_2SO_2$ as an internal standard).

complex unmodified after 72 h (Table 2). Minor degradation in the DMSO/$H_2O$ medium was associated with the release of *p*-cymene from $[4-6]^+$ and of acetic acid from $[4]^+$ and $[5]^+$ because of cleavage of the ester linkages. Interestingly, the *α*-diimine ligand and the bioactive fragment were not released from $[5]^+$ and $[6]^+$ (see the SI for details).

The initial molar conductivity values of $[1-3]NO_3$ in $H_2O$ ($\Lambda_m \approx 125$ S cm$^2$ mol$^{-1}$) are in the range of a 1:1 electrolyte[33] and are in accordance with the presence of intact cationic complexes $[1-3]^+$. Accordingly, the $^{35}$Cl NMR spectra, recorded on freshly prepared solutions in $H_2O$/MeOH (9:1, v/v; to increase the solubility of $[3]NO_3$), showed no evidence of free $Cl^-$ ions,[34] and the addition of NaCl (0.11 M) had no effect on the $^1$H NMR spectra. The quantity of $[1]^+$ and $[2]^+$ decreased progressively with time due to the formation of a secondary (*p*-cymene)Ru(*α*-diimine) species (less than 10%; $1^W$ and $2^W$; Figures S19 and S20), as indicated by the appearance of a new set of $^1$H resonances and a signal around 0 ppm in the $^{35}$Cl NMR spectra. In addition, a decrease in the pH (from 6.5 to 5.9–6.0) and an increase in the molar conductivity ($\Lambda_m \approx 160$ S cm$^2$ mol$^{-1}$) were detected, which is consistent with the occurrence of minor chloride/$H_2O$ replacement (eq 1), possibly followed by proton release from the $H_2O$ ligand in the resulting dicationic complex (eq 2).[35]

$$[(p\text{-cymene})RuCl(\alpha\text{-diimine})]^+(aq) + H_2O \rightarrow [(p\text{-cymene})Ru(H_2O)(\alpha\text{-diimine})]^{2+}(aq) + Cl^-(aq) \quad (1)$$

$$[(p\text{-cymene})Ru(H_2O)(\alpha\text{-diimine})]^{2+}(aq) \rightarrow [(p\text{-cymene})Ru(OH)(\alpha\text{-diimine})]^+(aq) + H^+(aq) \quad (2)$$

In contrast to $[1-3]^+$, both RAED[35,35] and RAPTA compounds[36] (Figure 1) are known to undergo rapid and extensive hydrolysis in $H_2O$, a feature that is considered to activate the complexes. Even the addition of 1 equiv of $AgNO_3$ to $[1-3]NO_3$ (in 9:1 $H_2O$/MeOH; see the SI) caused no change in their UV–vis and $^1$H NMR spectra, and AgCl precipitation was not observed. In comparison, the structurally related RAED compounds with 1,2-diamine ligands (Figure 1) undergo quantitative chloride/$H_2O$ displacement upon the addition of $Ag^+$, which is only partially reversed in a 0.1 M NaCl medium.[37]

Unlike $[1,2]NO_3$, a freshly prepared solution of $[3]NO_3$ in $H_2O$ has a rather low pH value (5.7), and the UV–vis spectrum quickly and reversibly changes when small volumes of NaOH(aq) or HCl(aq) are added in sequence. Consequently, an isosbestic point was detected at 437 nm (Figure S27) and could be related to the possible deprotonation of one phenolic group, resulting in the green-colored $3^B$ (Scheme 4a). A parallel $^1$H NMR spectroscopic study revealed chemical shift variations related to the aromatic *o*-CH ($\Delta\delta_H = -0.37$ ppm) and the imine HC=N ($\Delta\delta_H = -0.24$ ppm) groups, suggesting that $3^B$ experiences some delocalization of the negative charge over the *π* system of the **L3** ligand (Table S9 and Figure S29). A value of p$K_a$ = 7.7 ± 0.1 was determined for $[3]^+$ in a 0.1 M NaCl solution using a spectrophotometric method (see the Experimental Section), and therefore similar quantities of $[3]^+$ and its conjugate base $3^B$ are expected to be present in solution at physiological pH (≈7.4).

Basic solutions containing $[3]^+/3^B$ were not stable at room temperature, as indicated by changes in the UV–vis spectra and the appearance of a second set of signals in the $^1$H NMR spectra (Figure S28 and Tables S10 and S11). These variations become increasingly evident with increasing pH and are thus attributed to presumable $Cl^-/OH^-$ substitution, affording $[(\eta^6\text{-}p\text{-cymene})Ru(OH)\{\kappa^2N,N'\text{-}(HCN)_2(4\text{-}C_6H_4OH)(4\text{-}C_6H_4O)\}]$ ($3^{BW}$; Scheme 4b). In fact, ca. 70% of $3^{BW}$ was observed at pH ≈ 12 after a few minutes, accompanied by a sharp $^{35}$Cl NMR signal at ca. 0 ppm; conversely, red solutions containing $[3]NO_3$ at pH = 1.5–7 were stable for several days at room temperature, and no trace of $3^{BW}$ was detected by $^1$H NMR spectroscopy.

**Density Functional Theory (DFT) Study.** The observed stability of the metal–chloride bond in $[1-6]^+$ seems exceptional in the context of ruthenium(II) arene compounds, and potential anticancer compounds belonging to this family

**Scheme 4. Speciation of $[3]^+$ in $H_2O$: Acid–Base Equilibrium with the Formation of $3^B$ (Resonance Structures Are Shown in Figure S29) and Subsequent Ru–Cl Hydrolysis with the Formation of $3^{BW}$**

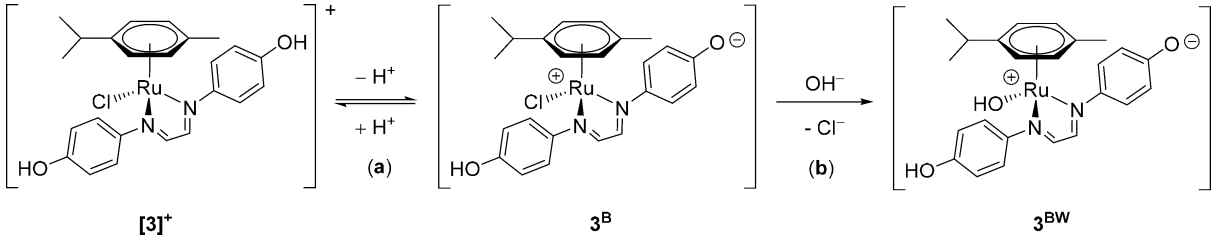




DOI: 10.1021/acs.inorgchem.8b00882
Inorg. Chem. XXXX, XXX, XXX–XXX

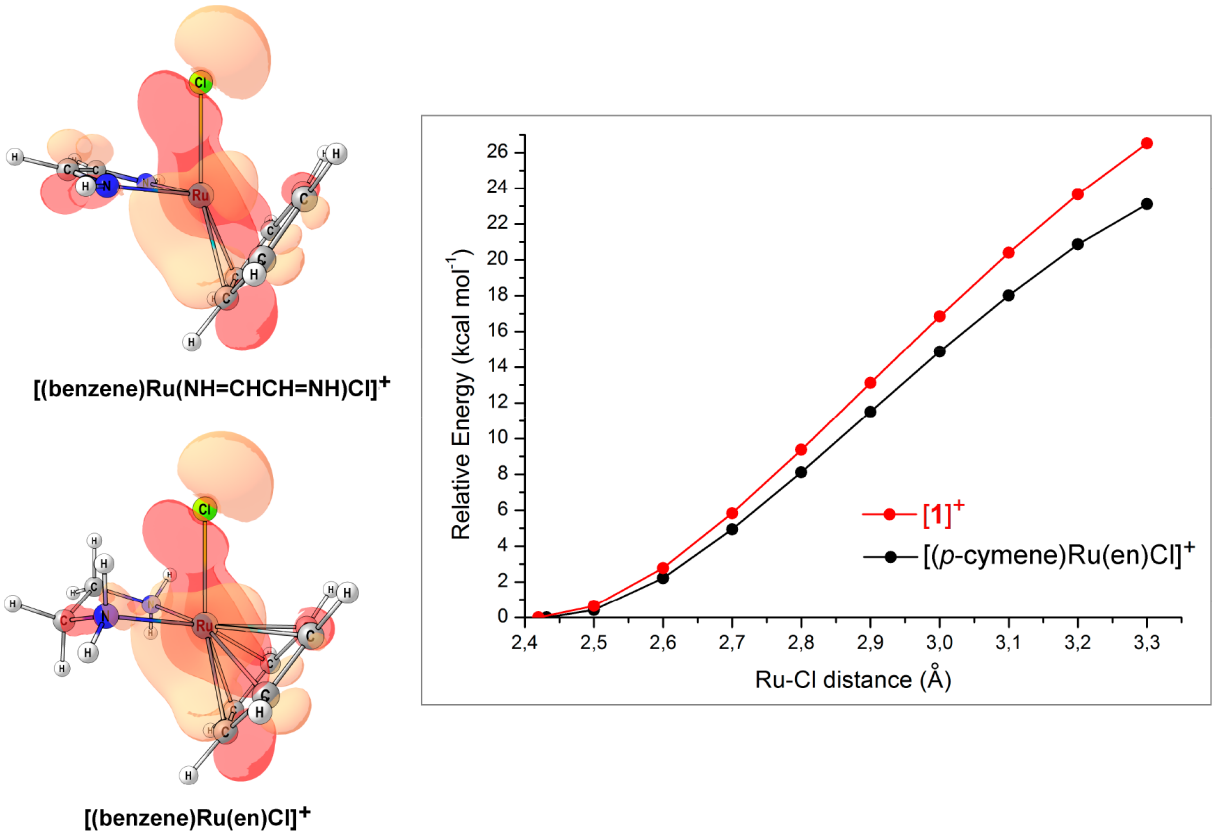


**Figure 3.** HOMO−2 molecular orbitals of $[(\eta^6\text{-benzene})Ru(NH{=}CHCH{=}NH)Cl]^+$ and $[(benzene)Ru(en)Cl]^+$ (surface isovalue = 0.035 au). Inset: Bond energy variation (kcal $mol^{-1}$) versus Ru−Cl distance for $[\mathbf{1}]^+$ and $[(p\text{-cymene})Ru(en)Cl]^+$. C-PCM/$\omega$B97X calculations and $H_2O$ as the continuous medium.

are usually believed to be readily activated by hydrolytic Ru−Cl cleavage (see above).

To rationalize this unusual stability, we carried out a DFT study to compare the Ru−Cl bond strength in $[\mathbf{1}]^+$, as a representative compound, with that in the structurally related RAED cation $[(\eta^6\text{-}p\text{-cymene})Ru(\kappa^2N\text{-en})Cl]^+$ (Figure 1). Chloride dissociation from the latter complex is more favorable with respect to $[\mathbf{1}]^+$ by 2.1 kcal $mol^{-1}$ [Gibbs free energy, conductor-like polarizable continuum model (C-PCM)/$\omega$B97X calculations, and $H_2O$ as the continuous medium]. The higher stability of the Ru−Cl bond in $[\mathbf{1}]^+$ is apparent from the plot of the bond energy upon variation of the Ru−Cl distance (see the inset in Figure 3). A comparative analysis of the occupied orbitals in the model compounds $[(\eta^6\text{-benzene})Ru(\kappa^2N\text{-}NH{=}CHCH{=}NH)Cl]^+$ and $[(\eta^6\text{-benzene})Ru(\kappa^2N\text{-}NHyCHyCHyNH_2)Cl]^+$ suggests that the different strength of the Ru−Cl bond is due to delocalization of the electron density on the lowest-energy $\pi^*$ orbital of the $\alpha$-diimine ligand. This feature is highlighted in particular by the HOMO−2 molecular orbitals of the two compounds (Figure 3), wherein ethylenediamine behaves as a $\sigma$ donor, while $\alpha$-diimine exhibits $\pi$ acidic behavior.

**Electrochemical Studies.**[38] Because the cytotoxicity of ruthenium compounds has often been associated with the occurrence of redox processes,[4] the electrochemical behavior of $[\mathbf{1}{-}\mathbf{3}]NO_3$ was investigated. Although $H_2O$ is the most obvious solvent with respect to biological studies, there is a paucity of electrochemical studies in aqueous media concerning $(\eta^6$-arene)Ru compounds evaluated for their possible anticancer activity.[39]

Previous electrochemical studies on $[(\eta^6\text{-}C_6H_6)RuCl\{\kappa^2N\text{-}(HCN^iPr)_2\}]$[11c] allowed the identification of both a reduction process (ca. −0.67 V) and an oxidation process (ca. +1.8 V) in a $CH_3CN$ solution, presumably favored by solvent coordination and by the redox noninnocent character of the $\alpha$-diimine ligand.[40]

The redox properties of $[\mathbf{1}{-}\mathbf{3}]NO_3$ were assessed by cyclic voltammetry (CV) with a glassy carbon (GC) electrode in an aqueous medium, and a parallel study was conducted on **L1** and $[\mathbf{1}]NO_3$ in a $CH_2Cl_2/[Bu_4N]PF_6$ solution. The peak potentials for the observed electron transfer are compiled in Table 3, and selected CV profiles are shown in Figures S30−S33.

Compounds $[\mathbf{1}{-}\mathbf{3}]NO_3$ in a phosphate buffer (PB) solution (pH = 7.3) displayed two independent redox processes, associated with reduction and oxidation processes of the complexes. The oxidation of $[\mathbf{1}{-}\mathbf{3}]NO_3$ occurs at potentials between +0.8 and +1.4 V; however, it is not followed by a reverse peak, indicating an irreversible process and leading to degradation of the compounds. During the cathodic scan, peaks were observed at −0.30, −0.34, and −0.20 V, which are associated with the reduction of $[\mathbf{1}]^+$, $[\mathbf{2}]^+$, and $[\mathbf{3}]^+$, respectively. For $[\mathbf{1}]NO_3$ and $[\mathbf{3}]NO_3$, this process was followed by a very intense reoxidation peak at ca. +0.14 V on the reverse scan. The high current peak intensity indicates an accumulation of the electrogenerated species on the surface of the electrode during the reduction step. In contrast, $[\mathbf{2}]^+$ displays a return peak of comparable current intensity occurring at a much lower potential (− 0.16 V; $\Delta E$ = 206 mV), and consequently the reduction process can be considered as quasi-


DOI: 10.1021/acs.inorgchem.8b00882
Inorg. Chem. XXXX, XXX, XXX−XXX

Table 3. Peak Potentials versus Normal Hydrogen Electrode for L1 and [1−3]$NO_3$ in Aqueous Media and a $CH_2Cl_2$ Solution

| | | reduction process[b] | | oxidation process[b] |
|---|---|---|---|---|
| compound | electrolyte[a] | $E_{pc}$/V | $E_{pa}$/V (return peak) | $E_{pa}$/V |
| **L1** | $CH_2Cl_2$/$[Bu_4N]PF_6$ | n.d. | n.d. | |
| [**1**]$NO_3$ | $CH_2Cl_2$/$[Bu_4N]PF_6$ | −0.707 | n.d. | n.d. |
| | PB/$H_2O$ (pH = 7.3) | −0.301 | +0.142[c] | +1.355 |
| | PB/$H_2O$ (pH = 7.3) + 0.1 M NaCl | −0.277 | +0.177[c] | +1.385 |
| [**2**]$NO_3$ | PB/$H_2O$ (pH = 7.3) | −0.362 | −0.156 | +1.43[d] |
| | PB/$H_2O$ (pH = 7.3) + 0.1 M NaCl | −0.342 | −0.142 | n.d. |
| [**3**]$NO_3$ | PB/$H_2O$ (pH = 7.3) | −0.200 | +0.148[c] | +0.864 |
| | AB/$H_2O$ (pH = 4.5) | −0.198 | −0.031 | +1.035 |

[a]PB = phosphate buffer; AB = acetate buffer. [b]Cathodic ($E_{pc}$) and anodic ($E_{pa}$) peak potentials measured at 0.1 V $s^{-1}$. [c]High peak current intensity. [d]The wave occurred at the upper limit of the potential window provided by the electrolyte. n.d. = not decteted.

reversible.[41] The addition of NaCl (0.1 M) to the solutions of [**1**]$NO_3$ and [**2**]$NO_3$ led to small variations in the respective CV profiles and peak potentials.

Because of the acid−base properties of [**3**]$NO_3$, CV was also conducted in an acetate buffer (AB) solution (pH = 4.5), where the complex remains mostly undissociated ($[\mathbf{3}]^+$; p$K_a$ = 7.7). The peak potential during the cathodic scan at pH = 4.5 is identical with that at pH = 7.3, thus in both cases related to the reduction of $[\mathbf{3}]^+$ (not $\mathbf{3}^B$). However, the reduction process assumed a quasi-reversible behavior at pH = 4.5 because the current intensity of the reverse peak is comparable, and the peak-to-peak separation ($\Delta E$) is 150 mV (vs 360 mV in a PB solution). Therefore, the different electrochemical behavior of [**3**]$NO_3$ in PB and AB solutions may be related to acid−base equilibria involving the reduced species [$\mathbf{3}^\bullet$].

From these data, the oxidation of [**1**−**3**]$NO_3$ in an aqueous solution at pH = 7.3 lies outside a biologically relevant range of potentials (−0.40 V < $E$ < +0.80 V;[42] see the SI). Conversely, the reduction of [**1**−**3**]$NO_3$ falls within such an electrochemical window. In comparison, CV of [**1**]$NO_3$ in $CH_2Cl_2$ showed an irreversible reduction process at a much lower potential (− 0.71 V), comparable to that reported for [($\eta^6$-$C_6H_6$)RuCl{$\kappa^2$-N-(HCN$^i$Pr)$_2$}] in MeCN (see above).[11c] Therefore, the aqueous medium plays a key role in making the reduction of $[\mathbf{1}]^+$ (and presumably of $[\mathbf{2}]^+$ and $[\mathbf{3}]^+$) more accessible (than in organic solvents).

The complexes could potentially undergo a reduction in the physiological environment, favored by the peculiar electronic properties of the $\alpha$-diimine ligand, which could contribute to their biological action.

**Cytotoxicity Studies.** The cytotoxicity of [**1**−**6**]X (X = Cl and $NO_3$), ligands **L1**−**L3**, and control compounds cisplatin, aspirin, and valproic acid was assessed against human ovarian carcinoma (A2780), human ovarian carcinoma with acquired cisplatin resistance (A2780cisR), and human embryonic kidney (HEK-293) cell lines (Table 4). **L1** and **L2** are inactive against all three cell lines, whereas **L3** is active in the mid-to-low micromolar range, with 2-fold selectivity observed toward the A2780 cell line. Interestingly, [**1**]$NO_3$, comprising inactive ligand **L1**, showed cytotoxicity in the low micromolar against all cell lines ($IC_{50}$ = ca. 2−4 $\mu$M), but no selectivity toward the cancer cell lines was observed.

Table 4. $IC_{50}$ Values ($\mu$M) of Ligands L1−L3, Complexes [**1**−**6**]X (X = Cl and $NO_3$), Bioactive Molecules (asp-$CO_2H$ and vp-$CO_2H$), and Cisplatin Used as a Control against A2780, A2780cisR, and HEK-293 Cell Lines after 72 h of Exposure[a]

| compound | A2780 | A2780cisR | HEK-293 |
|---|---|---|---|
| **L1** | >200 | >200 | >200 |
| **L2** | >200 | >200 | >200 |
| **L3** | 19 ± 1 | 25 ± 2 | 48 ± 1 |
| [**1**]$NO_3$ | 2.6 ± 0.6 | 3.9 ± 0.5 | 3.9 ± 0.5 |
| [**2**]$NO_3$ | >200 | >200 | >200 |
| [**3**]$NO_3$ | >200 | >200 | >200 |
| [**4**]Cl | 30 ± 3 | 54 ± 2 | 56 ± 3 |
| [**5**]$NO_3$ | 21 ± 2 | 18 ± 2 | 21 ± 3 |
| [**6**]$NO_3$ | 2.2 ± 0.3 | 3.7 ± 0.9 | 2.5 ± 0.9 |
| vp-$CO_2H$[43] | >1000 | >1000 | |
| asp-$CO_2H$[15c] | >200 | >200 | >200 |
| cisplatin | 2.0 ± 0.4 | 24 ± 3 | 8.9 ± 1.3 |

[a]Values are given as the mean ± standard deviation.

Complexes [**2**]$NO_3$ and [**3**]$NO_3$, containing **L2** and **L3**, respectively, were inactive against all cell lines, despite the cytotoxicity displayed by uncoordinated **L3**. Acetylation of the phenolic functions of [**3**]$NO_3$ significantly increases the cytotoxicity of the resulting complex [**4**]Cl; i.e., $IC_{50}$ goes from >200 $\mu$M to 30 ± 3 $\mu$M against the A2780 cell line.

A stronger effect is obtained when aspirin and valproic acid, which are both inactive against the three cell lines in their free (carboxylic acid) form, are tethered to the $[\mathbf{3}]^+$ scaffold; in particular, a marked increase in the cytotoxicity was observed for the valproate derivative [**6**]$NO_3$, compared to the parent [**3**]$NO_3$.

The octanol/$H_2O$ partition coefficients (log $P_{ow}$; Table 5) of the complexes were determined spectrophotometrically using the shlake-flask method (see the Experimental Section and SI), and the values tend to correlate with the observed cytotoxicities. Indeed, the least lipophilic complexes, [**2**]$NO_3$ and [**3**]$NO_3$, are also the least active of the series with $IC_{50}$ values of >200 $\mu$M. As the hydrophilicity decreases, the cytotoxicity of the complexes generally increases; complex [**1**]$NO_3$ is an outlier, with $IC_{50}$ values in the low micromolar range and a log $P_{ow}$ value of −0.78. The most hydrophobic complexes, [**5**]$NO_3$ and [**6**]$NO_3$, possessing log $P_{ow}$ values of >2.5, present $IC_{50}$ values in the mid-to-low micromolar range. This indicates that the aspirinate and valproate moieties might contribute to the cytotoxicity of the respective complexes mainly because of the lipophilicity that they provide.

Table 5. Partition Coefficients (log $P_{ow}$) of Ruthenium Compounds

| compound | solvent system | partition coefficient (log $P_{ow}$) |
|---|---|---|
| [**1**]$NO_3$ | 1-octanol/$H_2O$ | −0.78 |
| [**2**]$NO_3$ | 1-octanol/$H_2O$ | <−2.5 |
| [**3**]$NO_3$ | 1-octanol/$H_2O$ | −0.91 |
| | 1-octanol/PB solution | −0.64 |
| [**4**]Cl | 1-octanol/$H_2O$ | −0.26 |
| [**5**]$NO_3$ | 1-octanol/$H_2O$ | >2.5 |
| [**6**]$NO_3$ | 1-octanol/$H_2O$ | >2.5 |


DOI: 10.1021/acs.inorgchem.8b00882
Inorg. Chem. XXXX, XXX, XXX−XXX

Accordingly, the ester linkages connecting the bioactive fragments to the metal fragment appear quite stable in aqueous media (see above), possibly favoring uptake of the complexes into the cells.

## CONCLUSIONS

Ruthenium(II) arene complexes have been intensively investigated as future anticancer drugs, and promising results were previously obtained, among the others, with some derivatives containing N,N-bidentate ligands. Despite $\alpha$-diimines have been widely employed as robust N,N-bidentate ligands in coordination chemistry, ruthenium(II) arene-$\alpha$-diimine complexes were not considered to date for biological evaluation.

Herein, we have reported a series of new, $H_2O$-soluble, cationic (*p*-cymene)$Ru^{II}$ complexes with simple $\alpha$-diimines, unusually obtained as nitrate salts. The appropriate coordinated $\alpha$-diimine can be directly modified via esterification reactions, at the expense of the $H_2O$ solubility, without the need for protection/deprotection steps of the ruthenium(II) center. In general, the cytotoxicity of the complexes strongly depends on the nature of the $\alpha$-diimine N-substituents, including bioactive molecules tethered to it, resulting in some cases in $IC_{50}$ values in the low micromolar range.

As a consequence of the peculiar electron-withdrawing properties of the $\alpha$-diimine ligands, the complexes undergo only minor ruthenium chloride hydrolytic cleavage (rationalized by DFT calculations), and their electrochemical reduction in $H_2O$ falls within a biologically relevant range of potentials. In contrast, the prototype classes of anticancer compounds RAPTA and RAED are known to undergo rapid and extensive hydrolysis in $H_2O$, which is believed to activate the complexes.

## EXPERIMENTAL SECTION

**General Experimental Details.** All reagents and solvents were obtained from Alfa Aesar, Sigma-Aldrich, or TCI Europe and used without further purification. The following reagents were stored under $N_2$ as received: 4-aminophenol (4 °C, in the dark), aspirin (asp-$CO_2H$), valproic acid (vp-$CO_2H$), acetyl chloride, triethylamine (over 4 Å molecular sieves), 1,5-diazabicyclo[5.4.0]undec-7-ene (DBU; over 4 Å molecular sieves), and ethyl(diisopropylamino)carboxydiimide hydrochloride (EDCI·HCl; −20 °C). Glyoxal (40% w/w in $H_2O$) was stored at 4 °C. Compounds $[(\eta^6\text{-}p\text{-cymene})RuCl_2]_2$[44] and *N,N′*-bis(cyclohexyl)ethylenediimine (**L1**)[16] were prepared according to literature methods. The synthesis of [**4**−**6**]X (X = Cl and $NO_3$) was carried out under a $N_2$ atmosphere using standard Schlenk techniques and solvents distilled from the appropriate drying agents. All of the other operations were carried out in air with common laboratory glassware. Once isolated, all of the complexes were obtained as air-stable solids. NMR spectra were recorded on a Bruker Avance II DRX400 instrument equipped with a BBFO broad-band probe at 25 °C, unless otherwise specified. Chemical shifts (expressed in parts per million) are referenced to the residual solvent peaks[45] ($^1H$ and $^{13}C$) or to external standards ($^{14}N$ to $CH_3NO_2$ and $^{35}Cl$ to 1 M NaCl in $D_2O$).[46] In mixed solvents, chemical shifts were referenced to the residual peak of the major component as the pure solvent ($\delta_H$ = 2.50 ppm for DMSO in 9:1 DMSO-$d_6$/$D_2O$ and $\delta_H$ = 4.79 ppm for HDO in 9:1 $D_2O$/$CD_3OD$). Spectra were assigned with the assistance of DEPT-135 spectra and $^1H$−$^1H$ (COSY) and $^1H$−$^{13}C$ (gs-HSQC and gs-HMBC) correlation experiments.[47] IR spectra of solid samples were recorded on a PerkinElmer Spectrum One FT-IR spectrometer, equipped with a UATR sampling accessory. IR spectra of solutions were recorded on a PerkinElmer Spectrum 100 FT-IR spectrometer with a $CaF_2$ liquid transmission cell (4000−1000 $cm^{-1}$ range). UV−vis spectra were recorded on an Ultraspec 2100 Pro spectrophotometer. IR and UV−vis spectra were processed with *Spectragryph* software.[48] Carbon, hydrogen, and nitrogen analyses were performed on a Vario MICRO cube instrument (Elementar). Mass spectrometry (MS) spectra were obtained on a LTQ Orbitrap Elite (Thermo Fischer) in positive-ion mode. Melting points/decomposition temperatures were determined on a STMP3 Stuart scientific instrument with a capillary apparatus. pH measurements were performed with an Orion pH meter equipped with a Hamilton glass pH electrode, routinely calibrated with pH = 4.0 and 7.0 buffer solutions (Sigma-Aldrich). Conductivity measurements were carried out at 21 °C using an XS COND 8 instrument (cell constant = 1.0 $cm^{-1}$).[49]

The NMR ($^{14}N$, $^{35}Cl$) and molar conductivity data for reference compounds are given.

$NaNO_3$. $\Lambda_m$ (MeOH, $c = 1.7 \times 10^{-3}$ M) = 119 $S{\cdot}cm^2{\cdot}mol^{-1}$. $^{14}N$ NMR ($D_2O$): $\delta$ −5.0 ($\Delta\nu_{1/2}$ = 7 Hz). $^{14}N$ NMR ($CH_3OD$): $\delta$ −2.7 ($\Delta\nu_{1/2}$ = 14 Hz).

NaCl. $\Lambda_m$ (MeOH, $c = 3 \times 10^{-3}$ $mol{\cdot}L^{-1}$) = 85 $S{\cdot}cm^2{\cdot}mol^{-1}$. $^{35}Cl$ NMR ($CD_3OD$, acq. time 1 min): $\delta$ −28.3 ($\Delta\nu_{1/2} = 1.7 \times 10^2$ Hz).

$NH_4Cl$. $^{14}N$ NMR ($D_2O$): $\delta$ −360.7 ($\Delta\nu_{1/2}$ = 2 Hz). $^{14}N$ NMR ($CH_3OH/C_6D_6$ capillary): $\delta$ −366.1 ($\Delta\nu_{1/2}$ = 5 Hz).

$[Et_3NH]Cl$. $^{35}Cl$ NMR ($CD_3OD$, acq. time 1 min): $\delta$ −22.7 ($\Delta\nu_{1/2} = 2.3 \times 10^2$ Hz).

**Synthesis and Characterization of Compounds.** *N,N′-Bis(cyclohexyl)ethylenediimine (L1).* Compound **L1** (Chart 1) was prepared according to the literature:[16] pale-yellow solid, soluble in $Et_2O$, poorly soluble in DMSO. Anal. Calcd for $C_{14}H_{24}N_2$: C, 76.31; H, 10.98; N, 12.72. Found: C, 76.11; H, 10.76; N, 12.90. IR (solid state, $cm^{-1}$): 2922s, 2852s, 2793w, 2756w, 2657w, 1622s ($\nu_{C=N}$), 1468w, 1449m, 1443m-sh, 1435w-sh, 1371m, 1347m, 1321w, 1287m, 1260w-sh, 1252w, 1236w, 1182w, 1151w, 1063m, 1031w, 962m, 951s, 918w, 899w, 886s, 844m, 801w, 786w. UV−vis [$CH_2Cl_2$, $c = 1.0 \times 10^{-3}$ M; $\lambda_{max}$/nm ($\varepsilon/M^{-1}{\cdot}cm^{-1}$)]: 279 ($8.2 \times 10^2$). $^1H$ NMR ($CDCl_3$): $\delta$ 7.93 (s, 2H, C1−H), 3.15 (tt, $^3J_{HH}$ = 10.5 and 4.0 Hz, 2H, C2−H), 1.84−1.77 (m, 4H), 1.75−1.63 (m, 6H), 1.50 (ddd, $J$ = 15.1, 12.7, and 3.1 Hz, 4H), 1.34 (qt, $J$ = 12.4 and 3.2 Hz, 4H), 1.24 (tt, $J$ = 12.1 and 3.2 Hz, 2H). $^{13}C\{^1H\}$ NMR ($CDCl_3$): $\delta$ 160.2 (C1), 69.6 (C2), 34.1 (C3), 25.7 (C4), 24.8 (C5).

**Chart 1. Structure of L1**[a]

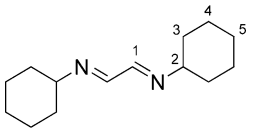


[a]The numbering refers to carbon atoms.

*N,N′-Bis(4-hydroxycyclohexyl)ethylenediimine (L2).* Glyoxal (40% w/w in $H_2O$, 0.40 mL, 3.5 mmol) and AcOH (50 $\mu$L, 0.87 mmol) were added to a suspension of *trans*-4-aminocyclohexanol (520 mg, 4.51 mmol) in $^i$PrOH (5 mL). The resulting pale-pink suspension was stirred at room temperature for 14 h. Therefore, the suspension was filtered, and the colorless solid was washed with $^i$PrOH (2 × 2 mL) and $Et_2O$ and then dried under vacuum (40 °C) over $P_2O_5$. Yield: 266 mg, 47%. *Alternative conditions*: MeOH, room temperature, 0% yield (no precipitation); MeOH, 50 °C, 27% yield; MeOH, reflux, 0% yield (dec); EtOH, room temperature, 40% yield; $^i$PrOH, room temperature, 2.5 h, 32%; THF, room temperature, 51% yield but product contains traces of *trans*-4-aminocyclohexanol. Compound **L2** (Chart 2) is soluble in MeOH and hot DMSO, poorly soluble in MeCN, EtOH, and $^i$PrOH, and insoluble in chlorinated solvents and $H_2O$.

**Chart 2. Structure of L2**[a]

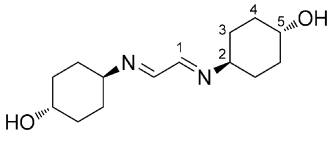


[a]The numbering refers to carbon atoms.



DOI: 10.1021/acs.inorgchem.8b00882
Inorg. Chem. XXXX, XXX, XXX−XXX

Anal. Calcd for $C_{14}H_{24}N_2O_2$: C, 66.63; H, 9.59; N, 11.10. Found: C, 66.30; H, 9.70; N, 11.22. IR (solid state, $cm^{-1}$): 3399m ($\nu_{O-H}$), 3332m ($\nu_{O-H}$), 2958m, 2946m, 2928m, 2903m, 2882m, 2859s, 1625s ($\nu_{C=N}$), 1454m-sh, 1444m, 1414w, 1372m, 1355m, 1334m, 1303m, 1289m, 1248w, 1218m, 1199w, 1124m, 1078s-sh, 1069s, 1036s, 1006m, 944s, 933s-sh, 901s, 886m. UV−vis [MeOH, $c = 3.6 \times 10^{-3}$ M; $\lambda_{max}$/nm ($\varepsilon$/$M^{-1}\cdot cm^{-1}$)]: 267 ($1.0 \times 10^3$). $^1$H NMR ($CH_3OD$): $\delta$ 7.91 (s, C1−H). $^1$H NMR (DMSO-$d_6$, 40 °C): $\delta$ 7.88 (s, 2H, C1−H), 4.49 (d, $^3J_{HH}$ = 4.4 Hz, 2H, OH), 3.49−3.37 (m, 2H, C5−H), 3.15 (ddd, $J$ = 14.3, 10.4, and 3.9 Hz, 2H, C2−H), 1.85 (dd, $J$ = 12.2 and 2.4 Hz, 4H, C4−H), 1.61 (dd, $J$ = 13.0 and 2.3 Hz, 4H, C3−H), 1.46 (dq, $J$ = 13.1 and 3.0 Hz, 4H, C3−H′), 1.26 (dq, $J$ = 12.9 and 3.1 Hz, 4H, C4−H′). $^{13}$C{$^1$H} NMR (DMSO-$d_6$, 40 °C): $\delta$ 156.0 (C1), 68.0 (C5), 67.6 (C2), 33.2 (C4), 31.6 (C3).

*N,N′-Bis(4-hydroxyphenyl)ethylenediimine (**L3**).* Compound **L3** (Chart 3) was prepared according to a modified literature procedure.[17]

**Chart 3. Structure of L3**[a]

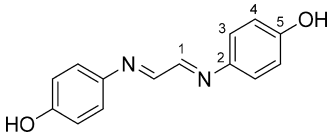


[a]The numbering refers to carbon atoms.

Glyoxal (40% w/w in $H_2O$, 0.65 mL, 5.7 mmol) and AcOH (0.10 mL, 1.7 mmol) were added to a suspension of 4-aminophenol (1.002 g, 9.18 mmol) in $^i$PrOH (14 mL). The resulting yellow suspension was stirred at 40 °C for 2.5 h under protection from light and then filtered. The resulting yellow solid was washed with $^i$PrOH (2 × 2 mL) and $Et_2O$, dried under vacuum (40 °C) over $P_2O_5$, and stored in the dark. Yield: 908 mg, 82%. *Alternative conditions*: MeOH, room temperature, 22 h, 63% yield; MeOH, reflux, 2 h, 83% yield; EtOH, room temperature, 22 h, 69% yield; $^i$PrOH, room temperature, 22 h, 72% yield. Compound **L3** is soluble in DMSO and MeOH, poorly soluble in acetone and MeCN, and insoluble in chlorinated solvents and $H_2O$. Anal. Calcd for $C_{14}H_{12}N_2O_2$: C, 69.99; H, 5.03; N, 11.66. Found: C, 69.60; H, 4.98; N, 11.80. IR (solid state, $cm^{-1}$): 3300−3000w-br ($\nu_{O-H}$), 3019m, 2988m, 2954m, 2902m, 2812m, 2743m, 2684m, 2603m, 2541w, 2513w, 2476w, 1888w, 1607s ($\nu_{C=N}$), 1592m-sh, 1574s, 1504s, 1453s, 1382m, 1330w, 1301w, 1269s, 1237s, 1200s, 1172s, 1158s, 1116m, 1104m, 1008w, 952w, 928w, 830s, 813s-sh, 794m-sh, 776s, 715m-sh. UV−vis [MeOH, $c = 3.0 \times 10^{-4}$ M; $\lambda_{max}$/nm ($\varepsilon$/$M^{-1}\cdot cm^{-1}$)]: 242 ($4.1 \times 10^4$), 296 ($2.5 \times 10^4$), 380 ($7.6 \times 10^4$). $^1$H NMR ($CH_3OD$): $\delta$ 8.36 (s, 2H, C1−H), 7.26 (d, $^3J_{HH}$ = 8.7 Hz, 4H, C3−H), 6.81 (d, $^3J_{HH}$ = 8.7 Hz, 4H, C4−H). $^{13}$C{$^1$H} NMR ($CH_3OD$): $\delta$ 157.5 (C1), 124.3 (C3), 117.1 (C4). $^1$H NMR (DMSO-$d_6$): $\delta$ 9.79 (s-br, 2H, OH), 8.40 (s, 2H, C1−H), 7.32 (d, $^3J_{HH}$ = 8.6 Hz, 4H, C3−H), 6.82 (d, $^3J_{HH}$ = 8.6 Hz, 4H, C4−H). $^{13}$C{$^1$H} NMR (DMSO-$d_6$): $\delta$ 157.8 (C5), 156.4 (C1), 141.2 (C2), 123.4 (C3), 115.9 (C4). $^1$H NMR ($CD_3CN$): $\delta$ 8.36 (s, 2H, C1−H), 7.29 (d, $^3J_{HH}$ = 8.4 Hz, 4H, C3−H), 7.20 (s, 2H, OH), 6.87 (d, $^3J_{HH}$ = 8.6 Hz, 4H, C4−H).

*[($\eta^6$-p-Cymene)RuCl{$\kappa^2$N-(HCN($C_6H_{11}$))$_2$}]$NO_3$ ([**1**]$NO_3$).* A suspension of [($\eta^6$-*p*-cymene)$RuCl_2$]$_2$ (201 mg, 0.328 mmol), $AgNO_3$ (113 mg, 0.665 mmol), and **L1** (147 mg, 0.667 mmol) in MeOH (6 mL) was stirred at room temperature for 5 h under protection from light. The resulting suspension (orange-red solution + colorless AgCl precipitate) was filtered over Celite. Volatiles were removed under vacuum from the filtrate solution, and the orange residue was suspended in $Et_2O$ (20 mL). The suspension was filtered, and the resulting crystalline orange solid was washed with $Et_2O$ and then dried under vacuum (40 °C). Yield: 337 mg, 93%. Compound [**1**]$NO_3$ (Chart 4) is soluble in $H_2O$, MeOH, acetone, and chlorinated solvents and insoluble in $Et_2O$ and hexane. Crystals suitable for X-ray diffraction were obtained from $CH_2Cl_2$ solutions of [**1**]$NO_3$ layered with heptane or hexane and settled aside at −20 °C. Anal. Calcd for $C_{24}H_{38}ClN_3O_3Ru$: C, 52.12; H, 6.92; N, 7.60. Found: C, 52.04; H, 6.81; N, 7.75. ESI-MS(+). Found: $m/z$ 491.1773 ([M]$^+$). Calcd for $C_{24}H_{38}ClN_2Ru^+$: $m/z$ 491.1770. $T_m$ = 112−115 °C (dec). IR (solid state, $cm^{-1}$): 3600−3300w-br, 3056w, 3040w, 2962w-sh, 2929m, 2856m, 1633w-br, 1537w ($\nu_{C=N}$), 1505w, 1470w-sh, 1452m, 1354s-sh, 1324s-br ($\nu_{NO_3}$), 1264m-sh, 1190w, 1160w, 1145w, 1090w, 1076m, 1054w, 1034w,1013w, 926w, 873m, 828w, 803w, 774w, 730w, 669w. UV−vis [$CH_2Cl_2$, $c = 1.0 \times 10^{-3}$ M; $\lambda_{max}$/nm ($\varepsilon$/$M^{-1}\cdot cm^{-1}$)]: 285 ($3.2 \times 10^3$), 368 ($2.3 \times 10^3$), 427 ($2.9 \times 10^3$). $\Lambda_m$ [$c$ = (1.0−2.0) × $10^{-3}$ M] = 18 $S\cdot cm^2\cdot mol^{-1}$ ($CH_2Cl_2$) and 113 $S\cdot cm^2\cdot mol^{-1}$ (MeOH). $^1$H NMR ($CDCl_3$): $\delta$ 8.34 (s, 2H, C8−H), 5.87 (d, $^3J_{HH}$ = 5.6 Hz, 2H, C4−H), 5.70 (d, $^3J_{HH}$ = 5.6 Hz, 2H, C3−H), 4.35 (t, $^3J_{HH}$ = 10.8 Hz, 2H, C9−H), 2.81 (hept, $^3J_{HH}$ = 6.7 Hz, 1H, C6−H), 2.51 (d, $^3J_{HH}$ = 11.3 Hz, 2H, C10−H), 2.34 (d, $^3J_{HH}$ = 11.1 Hz, 2H, C10′−H), 2.28 (s, 3H, C1−H), 1.96 (d, $^3J_{HH}$ = 13.0 Hz, 2H, C11−H*), 1.92−1.84 (m, 4H, C11−H*), 1.79−1.65 (m, 4H, C10′−H′ + C11−H*), 1.58−1.38 (m, 4H, C12−H), 1.29−1.22 (m, 4H, C10−H′ + C11−H*), 1.20 (d, $^3J_{HH}$ = 6.8 Hz, 6H, C7−H). Asterisks refer collectively to a proton attached to C11 or C11′. No change in the $^1$H NMR spectrum was observed after 14 days at room temperature. $^{13}$C{$^1$H} NMR ($CDCl_3$): $\delta$ 163.9 (C8), 108.9 (C5), 104.3 (C2), 87.3 (C4), 86.7 (C3), 75.9 (C9), 35.3 (C10), 33.4 (C10′), 31.8 (C6), 26.0 (C11/C11′), 25.6 (C11/C11′), 25.4 (C12), 22.4 (C7), 19.1 (C1).

**Chart 4. Structure of [1]$NO_3$**[a]

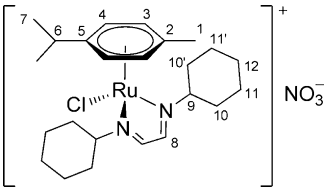


[a]The numbering refers to carbon atoms.

*[($\eta^6$-p-Cymene)RuCl($\kappa^2$N-{HCN(4-$C_6H_{10}OH$))$_2$}]$NO_3$ ([**2**]$NO_3$).* A brick-red suspension of [($\eta^6$-*p*-cymene)$RuCl_2$]$_2$ (104 mg, 0.170 mmol) and $AgNO_3$ (58 mg, 0.34 mmol) in MeCN (3 mL) was stirred at room temperature for 1 h under protection from light. The resulting suspension (yellow-orange solution + colorless AgCl precipitate) was filtered over Celite and the solid washed with MeCN. Compound **L2** (86 mg, 0.34 mmol) was added to the orange filtrate solution, and the mixture was stirred at reflux temperature for 3.5 h. Therefore, the red solution was cooled to room temperature, and volatiles were removed under vacuum. The residue was suspended in $Et_2O$ (20 mL) and then filtered. The resulting orange-brown solid was washed with $Et_2O$ and dried under vacuum (40 °C) over $P_2O_5$. Yield: 191 mg, 96%. On the other hand, a mixture of ruthenium compounds containing [**2**]$NO_3$ (Chart 5) was obtained when the reaction was carried out in MeOH at room temperature. Compound [**2**]$NO_3$ is soluble in $H_2O$, MeOH, and EtOH, less soluble in acetone, poorly soluble in $CH_2Cl_2$, and insoluble in $Et_2O$. Anal. Calcd for $C_{24}H_{38}ClN_3O_5Ru$: C, 49.27; H, 6.55; N, 7.18. Found: C, 49.04; H, 6.41; N, 7.23. ESI-MS(+). Found: $m/z$ 523.1667 ([M]$^+$). Calcd for $C_{24}H_{38}ClN_2O_2Ru^+$: 523.1665. IR (solid state, $cm^{-1}$): 3380m-br ($\nu_{O-H}$), 3054w, 2958m-sh, 2935m, 2905w, 2862m, 1648w-br, 1538w ($\nu_{C=N}$), 1504w, 1469m-sh, 1454m, 1377s, 1363s, 1321s-br ($\nu_{NO_3}$), 1305s, 1252m, 1229m, 1204m, 1161w, 1145w, 1121w, 1082s, 1062s,

**Chart 5. Structure of [2]$NO_3$**[a]

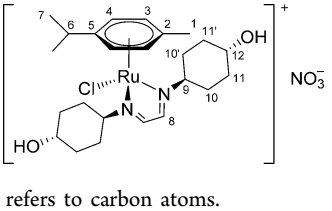


[a]The numbering refers to carbon atoms.



DOI: 10.1021/acs.inorgchem.8b00882
Inorg. Chem. XXXX, XXX, XXX−XXX

1040m-sh, 996w, 965m, 901w, 877m, 828m, 804w, 787w, 679w. UV–vis [MeOH, $c = 9.9 \times 10^{-4}$ M; $\lambda_{max}$/nm ($\varepsilon$/M$^{-1}$·cm$^{-1}$)]: 277 ($2.9 \times 10^3$), 372sh ($1.7 \times 10^3$), 426 ($2.8 \times 10^3$). $\Lambda_m$ (MeOH, $c = 9.9 \times 10^{-4}$ M) = 108 S·cm$^{-2}$·mol$^{-1}$. $^1$H NMR (DMSO-$d_6$): $\delta$ 8.38 (s, 2H, C8–H), 6.31 (d, $^3J_{HH}$ = 6.0 Hz, 2H, C4–H), 5.91 (d, $^3J_{HH}$ = 6.0 Hz, 1H, C3–H), 4.73 (d, $^3J_{HH}$ = 3.3 Hz, 2H, OH), 4.43 (t, $^3J_{HH}$ = 9.9 Hz, 2H, C9–H), 3.53–3.41 (m, 2H, C12–H), 2.69 (hept, $^3J_{HH}$ = 6.4 Hz, 1H, C6–H), 2.30 (d, $J$ = 12.4 Hz, 2H, C10–H), 2.16 (s, 3H, C1–H), 2.10 (d, $J$ = 12.3 Hz, 2H, C10′–H), 1.93 (d, $J$ = 10.8 Hz, 2H, C11′–H), 1.89–1.77 (m, 4H, C11–H + C10′–H′), 1.61–1.38 (m, 4H, C11–H′ + C11–H′), 1.27 (q, $J$ = 10.8 Hz, 2H, C10–H′), 1.05 (d, $^3J_{HH}$ = 6.6 Hz, 6H, C7–H). $^1$H NMR ($CD_3OD$): $\delta$ 8.33 (s, 2H, C8–H), 6.18 (d, $^3J_{HH}$ = 6.0 Hz, 2H, C4–H), 5.81 (d, $^3J_{HH}$ = 5.9 Hz, 2H, C3–H), 4.49 (t, $^3J_{HH}$ = 11.2 Hz, 2H, C9–H), 3.64 (t, $^3J_{HH}$ = 10.5 Hz, 2H, C12–H), 2.77 (hept, $^3J_{HH}$ = 6.7 Hz, 1H, C6–H), 2.52 (d, $J$ = 12.9 Hz, 2H, C10–H), 2.32–2.27 (m, 2H, C10′–H), 2.27 (s, 3H, C1–H), 2.13 (d, $J$ = 12.0 Hz, 2H, C11′–H), 2.04 (d, $J$ = 13.4 Hz, 2H, C11–H), 1.91 (q, $J$ = 11.4 Hz, 2H, C10′–H′), 1.62 (q, $J$ = 10.1 Hz, 2H, C11′–H′), 1.54 (q, $J$ = 10.1 Hz, 2H, C11–H′), 1.37 (q, $J$ = 11.2 Hz, 2H, C10–H′), 1.16 (d, $^3J_{HH}$ = 6.7 Hz, 6H, C7–H). No change in the $^1$H NMR spectrum was observed after 5 days at room temperature. $^{13}$C{$^1$H} NMR ($CD_3OD$): $\delta$ 165.3 (C8), 109.2 (C5), 108.4 (C2), 89.5 (C4), 87.3 (C3), 75.7 (C9), 70.1 (C12), 34.9 (C11), 34.5 (C11′), 34.0 (C10), 33.1 (C6), 32.1 (C10′), 22.7 (C7), 19.4 (C1).

*[($\eta^6$-p-Cymene)RuCl{$\kappa^2$N-(HCN(4-$C_6H_4OH$))$_2$}]$NO_3$ ([**3**]$NO_3$).* The first step of the synthesis was performed as described for [**2**]$NO_3$, using [($\eta^6$-*p*-cymene)$RuCl_2$]$_2$ (460 mg, 0.751 mmol), $AgNO_3$ (255 mg, 1.50 mmol), and MeOH (5 mL). Therefore, the suspension was filtered over Celite, and compound **L3** (360 mg, 1.50 mmol) was added to the orange filtrate solution, causing immediate darkening of the mixture. The solution was stirred at room temperature for 2 h, then volatiles were removed under vacuum. The residue was suspended in $Et_2O$ and then filtered. The resulting dark-red-brown solid was washed with $Et_2O$ and dried under vacuum (40 °C) over $P_2O_5$. Yield: 846 mg, 98%. Compound [**3**]$NO_3$ (Chart 6) is soluble in

**Chart 6. Structure of [3]$NO_3$[a]**

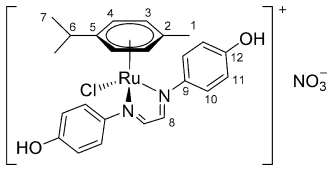


[a]The numbering refers to carton atoms.

$H_2O$, DMSO, MeOH, and acetone and insoluble in chlorinated solvents, $Et_2O$, and hexane. Anal. Calcd for $C_{24}H_{26}ClN_3O_5Ru$: C, 50.31; H, 4.57; N, 7.33. Found: C, 50.12; H, 4.68; N, 7.20. ESI-MS(+). Found: $m/z$ 511.0735 ([M]$^+$). Calcd for $C_{24}H_{26}ClN_2O_2Ru^+$: $m/z$ 511.0730. $T_m$ = 152–155 °C (dec). IR (solid state, cm$^{-1}$): 3560–3000m-br ($\nu_{O-H}$), 3064m, 2965m, 2879w, 2813w, 2692w, 2593w-br, 1604m ($\nu_{C=N}$), 1591m-sh, 1564m, 1504s, 1453m, 1370s, 1317s-br ($\nu_{NO_3}$), 1274s, 1227s, 1164s, 1107m, 1055w, 1035w, 1010w, 956w, 878w, 837s, 823m-sh, 805m-sh, 722w, 670w. UV–vis [MeOH$c = 1.0 \times 10^{-3}$ M; $\lambda_{max}$/nm ($\varepsilon$/M$^{-1}$·cm$^{-1}$)]: 268 ($1.3 \times 10^4$), 422 ($1.5 \times 10^4$), 550–575br ($3.4 \times 10^3$). $\Lambda_m$ (MeOH, $c = 1.0 \times 10^{-3}$ M) = 113 S·cm$^2$·mol$^{-1}$. $^1$H NMR (DMSO-$d_6$, 25 and 60 °C): broad resonances, $\delta$ 10.3 (br, 2H, OH), 8.47 (s-br, 2H, C8–H), 7.66 (s-br, 4H, C10–H), 6.98 (s-br, 4H, C11–H), 5.50 (s-br, 4H, C3–H + C4–H), 2.25* (s-br, C1–H), 0.95 (s-br, 6H, C7–H). Asterisks indicate peaks partially overlapped with the DMSO signal. $^1$H NMR ($CD_3OD$): $\delta$ 8.36 (s, 2H, C8–H), 7.69 (d, $^3J_{HH}$ = 8.3 Hz, 4H, C10–H), 6.99 (d, $^3J_{HH}$ = 8.3 Hz, 4H, C11–H), 5.47 (d, $^3J_{HH}$ = 6.1 Hz, 2H, C4–H), 5.42 (d, $^3J_{HH}$ = 6.1 Hz, 2H, C3–H), 2.39 (hept, $^3J_{HH}$ = 6.8 Hz, 1H, C6–H), 2.30 (s, 3H, C1–H), 1.05 (d, $^3J_{HH}$ = 6.9 Hz, 6H, C7–H). No variations in the $^1$H NMR spectrum were observed after 17 days at room temperature. $^{13}$C{$^1$H} NMR ($CD_3OD$): $\delta$ 163.2 (C8), 161.8 (C12), 146.2 (C9), 125.4 (C10), 117.0 (C11), 108.8 (C5), 107.8 (C2), 90.1 (C4), 89.3 (C3), 32.5 (C6), 22.2 (C7), 19.0 (C1).

*[($\eta^6$-p-Cymene)RuCl{$\kappa^2$N-(HCN(4-$C_6H_4OCOCH_3$))$_2$}]Cl ([**4**]Cl).* In a 25 mL Schlenk tube, DBU (0.10 mL, 0.67 mmol) was added to a suspension of [**3**]$NO_3$ (94 mg, 0.16 mmol) in $CHCl_3$ (10 mL). The dark-green reaction mixture was heated under reflux for 1 h, and then $CH_3COCl$ (50 $\mu$L, 0.70 mmol) was introduced. The resulting dark purple-red mixture was heated under reflux for 14 h and then allowed to cool to room temperature. The mixture was extracted with $H_2O$ (3 × 20 mL), and then volatiles were removed under vacuum from the organic phase. The residue was dissolved in a small volume of $Me_2CO$, and petroleum ether was added under stirring, causing precipitation of the title compound as a dark-brown solid. The suspension was filtered, and the solid was washed with $Et_2O$ and then dried under vacuum (40 °C). Yield: 71 mg, 68%. Compound [**4**]Cl (Chart 7) is soluble in

**Chart 7. Structure of [4]Cl[a]**

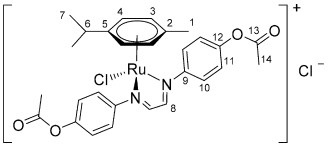


[a]The numbering refers to carton atoms.

DMSO, acetone, $CHCl_3$, poorly soluble in MeOH, and insoluble in $Et_2O$, hexane, and $H_2O$. Anal. Calcd for $C_{28}H_{30}ClN_3O_7Ru$: C, 51.18; H, 4.60; N, 6.40. Found: C, 51.18; H, 4.66; N, 6.48. ESI-MS(+). Found: $m/z$ 595.0941 ([M]$^+$). Calcd for $C_{28}H_{30}ClN_2O_4Ru^+$: $m/z$ 595.0942. IR (solid state, cm$^{-1}$): 3500w-br, 3060w, 2962w, 2933w, 2872w, 1890m-sh, 1860m, 1756s ($\nu_{C=O}$), 1622w, 1599w ($\nu_{C=N}$), 1494s, 1367s, 1269w, 1210s-sh, 1183s, 1161s, 1104m, 1041w, 1012s, 909m, 874w, 842m. IR ($CH_2Cl_2$, cm$^{-1}$): 1874w, 1765m ($\nu_{C=O}$), 1622w-sh, 1602m ($\nu_{C=N}$), 1497s, 1371m, 1215s-sh, 1194s, 1164m, 1015m. UV–vis [$CH_2Cl_2$, $c = 9.6 \times 10^{-4}$ M; $\lambda_{max}$/nm ($\varepsilon$/M$^{-1}$·cm$^{-1}$)]: 355 ($7.6 \times 10^3$), 440 ($4.5 \times 10^3$), 550–650br ($1.8 \times 10^3$). $\Lambda_m$ ($c = 9.6 \times 10^{-4}$ M) = 6.1 S·cm$^2$·mol$^{-1}$ ($CH_2Cl_2$), 60 S·cm$^2$·mol$^{-1}$ (MeOH). $^1$H NMR [$CDCl_3$ or 1:1 (v/v) $CDCl_3/CD_3OD$)]: broad resonances. $^1$H NMR ($CD_3OD$): $\delta$ 8.55 (s, 2H, C8–H), 7.85 (d, $^3J_{HH}$ = 8.6 Hz, 4H, C10–H), 7.40 (d, $^3J_{HH}$ = 8.6 Hz, 4H, C11–H), 5.58 (d, $^3J_{HH}$ = 6.2 Hz, 2H, C4–H), 5.48 (d, $^3J_{HH}$ = 7.0 Hz, 2H, C3–H), 2.43 (hept, $^3J_{HH}$ = 6.6 Hz, 1H, C6–H), 2.36 (s, 6H, C14–H), 2.27 (s, 3H, C1–H), 1.06 (d, $^3J_{HH}$ = 6.9 Hz, 6H, C7–H). Minor variations were observed in the $^1$H NMR spectrum of the solution maintained at room temperature for 2 months. $^{13}$C{$^1$H} NMR ($CD_3OD$): $\delta$ 171.0 (C13), 166.7 (C8), 153.9 (C12), 151.3 (C9), 124.8 (C10), 124.3 (C11), 110.3 (C5), 108.9 (C2), 90.4 (C4), 89.4 (C3), 32.6 (C6), 22.3 (C7), 20.9 (C14), 19.1 (C1). $^{14}$N NMR ($CD_3OD$; acq. time 14 h): no signal.

*[($\eta^6$-p-Cymene)RuCl{$\kappa^2$N-(HCN(4-$C_6H_4$OCO-asp))$_2$}]$NO_3$ ([**5**]$NO_3$).* In a 25 mL Schlenk tube, [**3**]$NO_3$ (110 mg, 0.192 mmol), DMAP (4 mg, 0.03 mmol), asp-$CO_2H$ (85 mg, 0.47 mmol), $CH_2Cl_2$ (7 mL), and EDCI·HCl (93 mg, 0.49 mmol) were introduced in this order, and the resulting dark-red suspension was stirred at room temperature. After 14 h, the reaction mixture was extracted with a $H_2O/NaNO_3$ 0.1 M solution (4 × 10 mL) and volatiles were removed under vacuum from the organic phase. The residue was suspended in $Et_2O$ and filtered; the resulting dark-brown solid was washed with $Et_2O$ and dried under vacuum (40 °C). Yield: 158 mg, 92%. The title compound could not be alternatively obtained via acyl chloride-mediated esterification: compound [**3**]$NO_3$ was completely unreactive toward asp-COCl/$Et_3N$ in a refluxing $CHCl_3$ or THF solution. Compound [**5**]$NO_3$ (Chart 8) is soluble in DMSO, acetone, and $CHCl_3$, less soluble in MeOH, and insoluble in $Et_2O$, hexane, and $H_2O$. Anal. Calcd for $C_{42}H_{38}ClN_3O_{11}Ru$: C, 56.21; H, 4.27; N, 4.68. Found: C, 56.01; H, 4.13; N, 4.70. ESI-MS(+). Found: $m/z$ 835.1375 ([M]$^+$). Calcd for $C_{42}H_{38}ClN_2O_8Ru^+$: $m/z$ 835.1369. IR (solid state, cm$^{-1}$): 3061w, 3036w, 2968w, 2934w, 2875w, 1762m-sh ($\nu_{C13=O}$), 1741s ($\nu_{C20=O}$), 1605m ($\nu_{C=N}$), 1580w, 1538w, 1494m, 1485m, 1452m,



DOI: 10.1021/acs.inorgchem.8b00882
Inorg. Chem. XXXX, XXX, XXX–XXX

**Chart 8. Structure of [5]$NO_3$**[a]

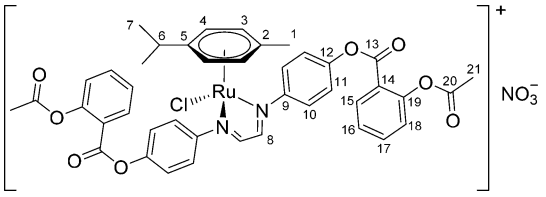

[a]The numbering refers to carbon atoms.

1367m, 1338m ($\nu_{NO_3}$), 1287m, 1244s, 1185s, 1161s, 1125m, 1109m, 1072m, 1047s, 1036s, 1011s, 962w, 915m, 875m, 832w, 807m, 751m, 700m. UV−vis [$CH_2Cl_2$, $c$ = 8.5 × $10^{-4}$ M; $\lambda_{max}$/nm ($\varepsilon$/$M^{-1}$·$cm^{-1}$)]: 273sh (1.6 × $10^4$), 357 (1.0 × $10^4$), 442 (3.3 × $10^3$), 550−600br (1.1 × $10^3$). $\Lambda_m$ ($c$ = 8.5 × $10^{-4}$ M) = 8.4 S·$cm^2$·$mol^{-1}$ ($CH_2Cl_2$), 67 S·$cm^2$·$mol^{-1}$ (MeOH). $^1$H NMR ($CDCl_3$): broad resonances. $^1$H NMR ($CD_3OD$): $\delta$ 8.58 (s, 2H, C8−H), 8.26 (dd, $^3J_{HH}$ = 7.8 Hz, $^4J_{HH}$ = 1.3 Hz, 2H, C15−H), 7.92 (d, $^3J_{HH}$ = 8.7 Hz, 4H, C10−H), 7.76 (dt, $^3J_{HH}$ = 7.8 Hz, $^4J_{HH}$ = 1.4 Hz, 2H, C17−H), 7.50 (d, $^3J_{HH}$ = 8.9 Hz, 4H, C11−H), 7.50−7.46 (m, 2H, C16−H), 7.29 (d, $^3J_{HH}$ = 8.1 Hz, 2H, C18−H), 5.62 (d, $^3J_{HH}$ = 6.4 Hz, 2H, C4−H), 5.52 (d, $^3J_{HH}$ = 6.4 Hz, 2H, C3−H), 2.47 (hept, $^3J_{HH}$ = 6.8 Hz, 1H, C6−H), 2.31 (s, 6H, C21−H), 2.29 (s, 3H, C1−H), 1.09 (d, $^3J_{HH}$ = 6.9 Hz, 6H, C7−H). Minor variations were observed in the $^1$H NMR spectrum of the solution maintained at room temperature for 3 days. $^{13}C\{^1H\}$ NMR ($CD_3OD$): $\delta$ 171.2 (C20), 166.8 (C8), 164.3 (C13), 153.7 (C12), 152.7 (C19), 151.6 (C9), 136.4 (C17), 133.1 (C15), 127.6 (C16), 125.3 (C18), 125.0 (C11), 124.4 (C10), 123.4 (C14), 110.3 (C5), 109.0 (C2), 90.4 (C4), 89.4 (C3), 32.6 (C6), 22.3 (C7), 21.0 (C21), 19.2 (C1). $^{14}$N NMR ($CD_3OD$): $\delta$ −3.1 ($\Delta\nu_{1/2}$ = 15 Hz, $NO_3^-$). $^{35}$Cl NMR ($CD_3OD$, acq. time 30′): no signal.

*[($\eta^6$-p-Cymene)RuCl{$\kappa^2$N-(HCN(4-$C_6H_4$OCO-vp))$_2$}]$NO_3$ ([**6**]$NO_3$).* The reaction was performed as described for [**5**]$NO_3$, using [**3**]$NO_3$ (97 mg, 0.17 mmol), DMAP (5 mg, 0.04 mmol), vp-$CO_2H$ (86 μL, 0.54 mmol), $CH_2Cl_2$ (7 mL), and EDCI·HCl (102 mg, 0.532 mmol). After 5 h, $H_2O$ (10 mL) was added to the dark-red suspension with vigorous stirring. The organic phase was then separated, and volatiles were removed under vacuum. The residue was dissolved in EtOAc/$Et_2O$ (1:1, v/v) and extracted with a 0.1 M $H_2O$/$NaNO_3$ solution (3 × 10 mL). Volatiles were removed under vacuum from the organic phase, and the residue was dissolved in a small volume of $Me_2CO$. The addition of petroleum ether under stirring caused precipitation of the title compound as a dark red-brown solid. The suspension was filtered; the solid was washed with petroleum ether and dried under vacuum (40 °C). Yield: 96 mg, 69%. Compound [**6**]$NO_3$ (Chart 9) is soluble

**Chart 9. Structure of [6]$NO_3$**[a]

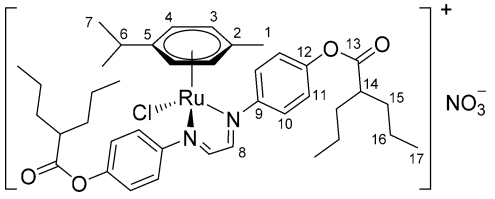

[a]The numbering refers to carbon atoms.

in MeCN (with decomposition), DMSO, EtOAc, and $CHCl_3$, poorly soluble in $Et_2O$, and insoluble in hexane and $H_2O$. Anal. Calcd for $C_{40}H_{54}ClN_3O_7Ru$: C, 58.21; H, 6.59; N, 5.09. Found: C, 58.20; H, 6.70; N, 5.11. ESI-MS(+). Found: $m/z$ 763.2836 ([M − Cl]$^+$). Calcd for $C_{40}H_{54}ClN_2O_4Ru^+$: $m/z$ 763.2810. IR (solid state, $cm^{-1}$): 3061w, 2958m, 2933m, 2872m, 1752s ($\nu_{C=O}$), 1654w, 1622w, 1599w ($\nu_{C=N}$), 1537w, 1494s, 1464m, 1371m-sh, 1336s ($\nu_{NO_3}$), 1190s, 1161s, 1147m-sh, 1124s-sh, 1101s, 1068m-sh, 1051m-sh, 1014m, 974w, 923w, 873m, 827m. UV−vis [$CH_2Cl_2$, $c$ = 9.2 × $10^{-4}$ M; $\lambda_{max}$/nm ($\varepsilon$/$M^{-1}$·$cm^{-1}$)]: 360 (1.0 × $10^4$), 440 (3.8 × $10^3$), 550−600br (1.4 × $10^3$). $\Lambda_m$ ($c$ = 9.2 × $10^{-4}$ M) = 7.8 S·$cm^2$·$mol^{-1}$ ($CH_2Cl_2$) and 90 S·$cm^2$·$mol^{-1}$ (MeOH). $^1$H NMR ($CD_3OD$): $\delta$ 8.52 (s, 2H, C8−H), 7.86 (d, $^3J_{HH}$ = 8.5 Hz, 4H, C10−H), 7.34 (d, $^3J_{HH}$ = 8.5 Hz, 4H, C11−H), 5.56 (d, $^3J_{HH}$ = 6.2 Hz, 2H, C4−H), 5.46 (d, $^3J_{HH}$ = 6.2 Hz, 2H, C3−H), 2.71 (m, $J$ = 14.1, 9.1, and 5.2 Hz, 2H, C14−H), 2.43 (hept, $^3J_{HH}$ = 6.8 Hz, 1H, C6−H), 2.24 (s, 3H, C1−H) 1.84−1.73 (m, 4H, C15−H), 1.68−1.59 (m, 4H, C15−H′), 1.49 (sex, $^3J_{HH}$ = 7.2 Hz, 8H, C16−H), 1.05 (d, $^3J_{HH}$ = 6.9 Hz, 6H, C7−H), 1.02 (t, $^3J_{HH}$ = 7.3 Hz, 12H, C17−H). $^{13}C\{^1H\}$ NMR ($CD_3OD$): $\delta$ 176.2 (C13), 166.6 (C8), 153.8 (C12), 151.3 (C9), 124.9 (C10), 124.1 (C11), 110.3 (C5), 108.6 (C2), 90.2 (C4), 89.4 (C3), 46.5 (C14), 35.7 (C15), 32.5 (C6), 22.3 (C7), 21.7 (C16), 19.1 (C1), 14.4 (C17). $^{14}$N NMR ($CD_3OD$): $\delta$ −2.9 ($\Delta\nu_{1/2}$ = 19 Hz, $NO_3^-$).

**X-ray Crystallography.** Crystal data and collection details for [**1**]$NO_3$ are reported in Table 6. Data were recorded on a Bruker

**Table 6. Crystal Data and Measurement Details for [1]$NO_3$**

| | |
|---|---|
| formula | $C_{24}H_{38}ClN_3O_3Ru$ |
| fw | 553.09 |
| $T$, K | 100(2) |
| $\lambda$, Å | 0.71073 |
| cryst syst | monoclinic |
| space group | $P2_1/c$ |
| $a$, Å | 11.6812(7) |
| $b$, Å | 11.5991(7) |
| $c$, Å | 18.3969(10) |
| $\beta$, deg | 100.709(2) |
| cell volume, Å$^3$ | 2449.2(2) |
| $Z$ | 4 |
| $D_c$, g·$cm^{-3}$ | 1.500 |
| $\mu$, $mm^{-1}$ | 0.780 |
| $F$(000) | 1152 |
| cryst size, mm | 0.15 × 0.13 × 0.09 |
| $\theta$ limits, deg | 1.774−25.050 |
| reflns collected | 28912 |
| indep reflns | 4327 [$R_{int}$ = 0.1359] |
| data/restraints/param | 4327/228/290 |
| GOF on $F^2$ | 1.171 |
| $R_1$ [$I > 2\sigma(I)$] | 0.0850 |
| $wR_2$ (all data) | 0.1648 |
| largest diff peak/hole, e·Å$^{-3}$ | 1.709/−2.360 |

APEX II diffractometer equipped with a Photon 100 detector using Mo K$\alpha$ radiation. Data were corrected for Lorentz polarization and absorption effects (empirical absorption correction *SADABS*).[50] The structure was solved by direct methods and refined by full-matrix least squares based on all data using $F^2$.[51] Hydrogen atoms were fixed at calculated positions and refined by a riding model. All non-hydrogen atoms were refined with anisotropic displacement parameters.

**Solubility and Stability Studies.** All measurements (pH, UV−vis, NMR, and conductivity) were performed at room temperature. The molar conductivity ($\Lambda_m$) and molar absorption coefficients ($\varepsilon$) were calculated with respect to the starting material. Molar percent values of the compounds in solution are based on $^1$H NMR spectroscopy and refer to identified compounds only (indicated as % NMR) or to $Me_2SO_2$ used as an internal standard (indicated as % NMR vs internal standard).[32] NMR signals in braces indicate superimpositions with other species. The solubility (S/M, at 21 °C) was calculated on saturated $D_2O$ solutions by $^1$H NMR with respect to $Me_2SO_2$ (internal standard).

Data are reported for each compound (Tables S2−S8 and Figures S19−S25); selected data are compiled in Table 2.

*General Procedure ($D_2O$ Solution).* The compound ([**1**−**3**]$NO_3$, 0.10 mmol) was suspended in a $D_2O$ solution (1.0 mL) containing $Me_2SO_2$ [$c$ = 7.1 × $10^{-3}$ mol·$L^{-1}$; $\delta$ 3.13 (s, 6H) in $D_2O$] and stirred at


DOI: 10.1021/acs.inorgchem.8b00882
Inorg. Chem. XXXX, XXX, XXX−XXX

21 °C for 24 h. An aliquot (0.50 mL) of the resulting saturated solution was transferred to an NMR tube and analyzed by $^1$H NMR spectroscopy. The solution was kept at 37 °C for 72 h and at 21 °C for at least 6 days. After each period, the solution was analyzed by $^1$H and $^{35}$Cl NMR spectroscopy. Finally, NaCl (50 μL of a 1.0 M solution in $D_2O$, $c_{NaCl}$ = 0.1 M) was added and the $^1$H spectrum repeated. Parallel experiments were carried out on dilute solutions ($c_{Ru}$ = 1.0 × 10$^{-3}$ M), which were kept at 37 °C for 72 h. The molar conductivity ($\Lambda_m$), pH, and UV−vis spectra were recorded immediately after dissolution and at the end of this period. See Figures S19−S21 and Tables S2−S4 for details.

*General Procedure (DMSO-$d_6$/$D_2O$ Solution).* The compound ([**3**−**6**]X, where X = Cl and $NO_3$) was dissolved in a 9:1 (v/v) DMSO-$d_6$/$D_2O$ solution (1.0 mL; [Ru] = 1.5 × 10$^{-2}$ mol·L$^{-1}$) containing $Me_2SO_2$ [$c$ = 5.5 × 10$^{-3}$ mol·L$^{-1}$; $\delta$ 2.97 (s, 6H) in 9:1 (v/v) DMSO-$d_6$/$D_2O$]. An aliquot of the resulting solution (0.60 mL) was transferred to a NMR tube, maintained at 37 °C for 72 h, and analyzed by $^1$H NMR spectroscopy as a function of time ($^{35}$Cl NMR analysis was performed at the end of the experiment). The remaining solution was diluted up to 4.0 mL with 9:1 (v/v) DMSO/$H_2O$ (final [Ru] = 1.5 × 10$^{-3}$ mol·L$^{-1}$), maintained at 37 °C for 72 h and analyzed by conductivity and UV−vis spectroscopy as a function of time. All measurements (NMR, conductivity, and UV−vis) were performed upon a brief cooling to ambient temperature, and then Ru-containing solutions were heated again at 37 °C. See Figures S22−S25 and Tables S5−S8 for details.

**Speciation of [3]$NO_3$ in $H_2O$ at Different pH Values: Acid Dissociation and Hydrolysis.** All operations were carried out at room temperature. NaOH and HCl solutions in $H_2O$ were prepared from a 1.0 M Normex solution (Carlo Erba) and standardized by titration before use.

*UV−Vis Measurements.* To a graduated 5 mL flask were added [**3**]$NO_3$ (2.50 mL of a 1.75 × 10$^{-3}$ M solution in $H_2O$) and NaCl (0.50 mL of a 1.0 M solution in $H_2O$), followed by the appropriate amount of NaOH (3.37 × 10$^{-3}$ or 1.0 M) or HCl (1 × 10$^{-2}$ or 1.0 M) and then $H_2O$ up to a constant volume (5.0 mL). The resulting red/green solutions ($c_{Ru}$ = 8.75 × 10$^{-4}$ M; $I$ = 0.1 M)[52] were stirred for 10 min at room temperature, then the pH value was measured (pH = 1.57−12.2), and their UV−vis spectra were recorded. The solutions were maintained at room temperature for 20 h, and their UV−vis spectrum and pH measurement were repeated.

*NMR Measurements.* Progressively increasing amounts of KOH (0−0.80 μL; 0.19 M solution in $D_2O$) were added to a solution of [**3**]$NO_3$ in $D_2O$ (4.0 mL; $c_{Ru}$ = 4.4 × 10$^{-3}$ M). After each addition, the pH* of the solution was measured, and an aliquot (0.50 mL) of the same was transferred to an NMR tube. The pD was calculated according to the equation pD = pH* + 0.4,[53] where pH* is the reading of the $H_2O$-calibrated pH meter (pD = 7.17−11.8). Within 30 min from the addition of KOH, $^1$H and $^{35}$Cl NMR spectra of each solution were recorded. Therefore, the solutions were maintained at room temperature for 62 h, and a new $^1$H NMR spectrum was registered.

*NMR and UV−Vis Characterization of [3]$^+$ and $\mathbf{3^B}$.* Solutions of [**3**]$NO_3$ in $H_2O$ underwent instantaneous and reversible UV−vis variations upon the addition of NaOH or HCl in the pH range 1−10. Furthermore, a single set of pH-dependent $^1$H resonances were observed in the $^1$H NMR spectra (except for the most basic solutions, see onward). These features are consistent with an acid−base equilibrium (acid, [**3**]$^+$; base, $\mathbf{3^B}$; see Scheme 4). Plots of UV−vis spectra for [**3**]$NO_3$/$H_2O$ solutions at different pH values are given in Figures S27 and S28. $^1$H NMR resonances of [**3**$^+$]/$\mathbf{3^B}$ at different pH values are compiled in Table S9. Selected UV−vis and NMR data are reported below (the same atom numbering as [**3**]$NO_3$ is used; see Chart 6).

pH = 5.25: red solution, major species [**3**]$^+$. UV−vis [$\lambda_{max}$/nm ($\varepsilon$/M$^{-1}$·cm$^{-1}$)]: 266 (8.3 × 10$^3$), 415 (1.3 × 10$^4$), 540−560 (2.6 × 10$^3$). pH = 9.27: green solution, major species $\mathbf{3^B}$. UV−vis [$\lambda_{max}$/nm ($\varepsilon$/M$^{-1}$·cm$^{-1}$)]: 240sh (1.5 × 10$^4$), 283 (9.0 × 10$^3$), 364 (4.8 × 10$^3$), 468 (1.2 × 10$^4$), 610sh (1.3 × 10$^4$), 638 (1.4 × 10$^4$). pD = 11.8: dark-green solution. $^1$H NMR ($D_2O$, $\mathbf{3^B}$): $\delta$ 8.17 (s, 2H, C8−H), 7.59 (d, $^3J_{HH}$ = 9.0 Hz, 4H, C10−H), 6.70 (d, $^3J_{HH}$ = 8.7 Hz, 4H, C11−H), 5.59 (d, $^3J_{HH}$ = 6.9 Hz, 2H, C4−H), 5.51 (d, $^3J_{HH}$ = 6.2 Hz, 2H, C3−H), 2.33 (s, 3H, C1−H), 0.99 (d, $^3J_{HH}$ = 6.8 Hz, 6H, C7−H).

*Determination of p$K_a$.*[54] UV−vis spectra of freshly prepared [**3**]$NO_3$/$H_2O$ solutions with pH in the range 5.25−10.80 displayed an isosbestic point ($\lambda$ = 437 nm; Figure S27) and were used for the determination of p$K_a$ of [**3**]$^+$, according to a previously published method.[55] Briefly, values of $y$ = log[($A$ − $A^{acid}$)/($A^{basic}$ − $A$)] were calculated, where $A$ is the absorbance of the selected solution at a given wavelength and $A^{acid}$ and $A^{basic}$ represent the absorbance at the lowest (5.25) and highest (10.80) pH values at the same wavelength. Least-squares linear regression of (pH; $y$) data gave an equation of the type $y$ = $a$pH + $b$; therefore, p$K_a$ could be calculated as p$K_a$ = −$b$/$a$. The procedure was repeated at four different wavelengths (two before and two after the isosbestic point), and the results were averaged, affording p$K_a$ = 7.7 ± 0.1.

*pH-Dependent Behavior of [3]$NO_3$ and the Formation of [($\eta^6$-p-Cymene)Ru(OH){$\kappa^2$N,N′-(HCN)$_2$(4-C$_6$H$_4$OH)(4-C$_6$H$_4$O)}] ($\mathbf{3^{BW}}$) in Basic Solutions.* The stability of [**3**]$NO_3$/$H_2O$ solutions at room temperature for 20 or 62 h at different pH/pD values was evaluated by UV−vis and $^1$H NMR spectroscopy. Variations in the UV−vis spectra as well as the appearance of a second set of $^1$H signals were attributed to the formation of $\mathbf{3^{BW}}$ from $\mathbf{3^B}$, upon Ru−Cl hydrolysis (Scheme 4). Data and observations are compiled in Tables S10 and S11. The amount of $\mathbf{3^{BW}}$ in solution (as percent molar ratio with respect to [**3**]$^+$ + $\mathbf{3^B}$) as a function of time was calculated from the $^1$H NMR spectrum. The NMR data for $\mathbf{3^{BW}}$ are given below (pD = 11.8; the same atom numbering as [**3**]$NO_3$ is used; see Chart 6). $^1$H NMR ($D_2O$): $\delta$ 8.22 (s, 2H, C8−H), 7.54 (d, $^3J_{HH}$ = 8.9 Hz, 4H, C10−H), 6.71 (d, $^3J_{HH}$ = 8.7 Hz, 4H, C11−H), 5.47 (d, $^3J_{HH}$ = 6.1 Hz, 2H, C4−H), 5.38 (d, $^3J_{HH}$ = 6.0 Hz, 2H, C3−H), 2.32 (s, 3H, C1−H), 0.90 (d, $^3J_{HH}$ = 6.8 Hz, 6H, C7−H). $^{35}$Cl NMR ($D_2O$, acq. time 10 min): $\delta$ 0.18 ($\Delta\nu_{1/2}$ = 9 Hz, Cl$^-$).

**Determination of Partition Coefficients (log $P_{ow}$).** Partition coefficients ($P_{ow}$; IUPAC, $K_D$ partition constant[56]), defined as $P_{ow}$ = $c_{org}$/$c_{aq}$, where $c_{org}$ and $c_{aq}$ are the molar concentrations of the selected compound in the organic and aqueous phase, respectively, were determined by the shake-flask method[57] and UV−vis measurements. Values of log $P_{ow}$ for compounds [**1**−**5**]$NO_3$ and [**6**]Cl are compiled in Table 5. All of the operations were carried out at 21 ± 1 °C. Deionized $H_2O$ and 1-octanol were mixed and vigorously stirred for 24 h at room temperature to allow saturation of both phases, then separated by centrifugation, and used for the following experiments. 1-Octanol-saturated PB solution ($Na_2HPO_4$/$KH_2PO_4$, $\sum c_{PO_4}$ = 50 mM, pH = 7.3) was prepared analogously. A solution of the selected ruthenium compound ([**1**−**3**]$NO_3$) in the aqueous phase ($V$ = 20 mL) was prepared, and its UV−vis spectrum was recorded. An aliquot of the solution ($V_{aq}$ = 3.0 mL) was then transferred into a test tube, and the organic phase ($V_{org}$ = 3.0 mL) was added. The mixture was vigorously stirred for 2 h, and the resulting emulsion was centrifuged (2000 rpm, 15 min) to separate the phases. Hence, the UV−vis spectrum of the aqueous phase was recorded. The partition coefficient was then calculated following the method described in the Supporting Information. An analogous procedure was followed for compounds [**4**]Cl and [**5**−**6**]$NO_3$, which were initially dissolved in the organic phase ($V$ = 20 mL). UV−vis measurements were carried out using 1 cm quartz cuvettes. The wavelength of the maximum absorption of each compound was used for UV−vis quantification ($\lambda_{max}$ = 420 nm for [**1**−**3**]$NO_3$ and 360 nm for [**4**]Cl and [**5**−**6**]$NO_3$). Solutions of the ruthenium compound in the aqueous or organic phase ([Ru] ≈ 5 × 10$^{-4}$ M for [**1,2**]$NO_3$; [Ru] ≈ 1.5 × 10$^{-4}$ M for [**3**−**6**]X, where X = Cl and $NO_3$) were prepared so as to give absorbance values of around 1.2−1.5 at $\lambda_{max}$.

**Computational Studies.** The electronic structures of the compounds were optimized using the range-separated ωB97X DFT functional[58] in combination with Ahlrichs' split-valence-polarized basis set, with an effective core potential on the ruthenium center.[59] The C-PCM implicit solvation model was added to ωB97X calculations, considering $H_2O$ as a continuous medium.[60] The stationary points were characterized by IR simulations (harmonic approximation), from


DOI: 10.1021/acs.inorgchem.8b00882
Inorg. Chem. XXXX, XXX, XXX−XXX

which zero-point vibrational energies and thermal corrections ($T$ = 25 °C) were obtained.[61] The software used was *Gaussian 09*.[62]

**Electrochemistry.** CV measurements were performed at 24 ± 1 °C with a PalmSens4 instrument interfaced to a computer employing *PSTrace5* electrochemical software. All potentials are reported versus normal hydrogen electrode (NHE). Current sign convention adopted: negative currents/cathodic process; positive currents/anodic process. Peak potentials for compounds [**1**−**3**]$NO_3$ and **L1** are compiled in Table 3, and cyclic voltammograms are given in Figures S30−S33.

*Experiments in Aqueous Media.* PB ($Na_2HPO_4/KH_2PO_4$, $\sum c_{PO_4}$ = 50 mM, pH = 7.3) and AB (NaOAc/AcOH, $\sum c_{AcO}$ = 0.21 M, pH = 4.5) solutions were prepared in ultrapure $H_2O$ and used as supporting electrolytes. The three-electrode home-built cell was equipped with a platinum sheet counter electrode, a Teflon-encapsulated GC working electrode (BASi, diameter 3 mm), and a leak-free 3.4 M Ag/AgCl/KCl reference electrode (eDAQ). The supporting electrolyte (5.0 mL) was introduced into the cell and deareated by argon bubbling for some minutes. The working electrode was cycled several times between the cathodic and anodic limits (−1.15/+1.55 and −1.05/+1.71 V for PB and AB solutions, respectively) until there was no change in the charging current. The analyte was then introduced ($c \approx 7 \times 10^{-4}$ M), and voltammograms were recorded (scan rate: 0.1 V·s$^{-1}$). NaCl (30 mg, 0.10 M) was then added to the solution, and the voltammograms were repeated.

The reference electrode was calibrated against a HydroFlex hydrogen reference electrode (eDAQ) placed in a 1.00 M HCl solution (thus acting as a NHE).[63] Prior to measurements, the GC working electrode was polished by the following procedure:[64] manual rubbing with a 0.3 $\mu$M $Al_2O_3$ slurry in $H_2O$ (eDAQ) for 2 min, then sonication in ultrapure $H_2O$ for 10 min, manual rubbing with a 0.05 $\mu$M $Al_2O_3$ slurry in $H_2O$ (eDAQ) for 2 min, and then sonication in ultrapure $H_2O$ for 10 min. The three-electrode cell was routinely checked by measuring $E_{1/2}$ and $\Delta E$ of the $Fe(CN)_6^{3-}/Fe(CN)_6^{4-}$ couple in the PB solution.[65]

*Experiments in Dichloromethane.* HPLC-grade dichloromethane (Sigma-Aldrich) was stored under argon over 3 Å molecular sieves. [$^n$Bu$_4$N][$PF_6$] (Fluka, electrochemical grade) and $Cp_2Fe$ (Fluka) were used without further purification. CV measurements were carried out under argon using 0.2 M [$^n$Bu$_4$N][$PF_6$] in $CH_2Cl_2$ as the supporting electrolyte. The working and counter electrodes consisted of a platinum disk and a platinum gauze, respectively. A platinum quasi-reference electrode was employed as a reference. The three-electrode home-built cell was predried by heating under vacuum and filled with argon. The Schlenk-type construction of the cell maintained anhydrous and anaerobic conditions. The solution of supporting electrolyte was introduced into the cell, and the working electrode was cycled several times between the cathodic and anodic limits (−2.88/+1.71 V vs NHE, respectively) until there was no change in the charging current. The analyte was then introduced ($c \approx 7 \times 10^{-4}$ M), and the voltammograms were recorded (scan rate: 0.1 V·s$^{-1}$); then a small amount of ferrocene was added, and the voltammograms were repeated. The potentials were determined by placing $E_{1/2}$ = +0.39 V versus saturated calomel electrode (SCE) for the $Cp_2Fe^+/Cp_2Fe$ couple (as experimentally determined for our home-built cell)[66] and then referenced to NHE ($E_{SCE}$ = +0.241 V vs NHE).[42]

**Cell Culture and Cytotoxicity Studies.** Human ovarian carcinoma (A2780 and A2780cisR) cell lines were obtained from the European Collection of Cell Cultures (ECACC, U.K.). The nontumoral human embryonic kidney (HEK-293) cell line was obtained from ATCC (Sigma, Switzerland). RPMI-1640 GlutaMAX and DMEM GlutaMAX media were obtained from Life Technologies (Switzerland), fetal bovine serum (FBS) was obtained from Sigma, a penicillin/streptomycin solution was obtained from Life Technologies, and cisplatin was obtained from TCI.

The cells were routinely cultured in RPMI-1640 GlutaMAX (A2780 and A2780cisR) and DMEM GlutaMAX (HEK-293) media containing 10% heat-inactivated FBS and a 1% penicillin/streptomycin solution at 37 °C and $CO_2$ (5%). The A2780cisR cell line were routinely treated with cisplatin (2 $\mu$M) in the medium.

The cytotoxicity of the compounds was determined using 3-(4,5-dimethyl-2-thiazolyl)-2,5-diphenyl-2*H*-tetrazolium bromide (MTT) assay.[67] Cells were seeded in flat-bottomed 96-well plates as a suspension in a medium containing 10% heat-inactivated FBS and a 1% penicillin/streptomycin solution (100 $\mu$L and approximately 4300 cells·well$^{-1}$) and incubated for 24 h. Stock solutions of compounds were prepared in DMSO, or Milli-Q water in the case of [**2**]$NO_3$ and [**3**]$NO_3$, and were rapidly diluted in the medium. The solutions were sequentially diluted (final DMSO concentration of 0.5%) to give a compound concentration range (0−500 $\mu$M). Cisplatin was included as a positive control (0−100 $\mu$M). The compounds were added to the preincubated 96-well plates in 100 $\mu$L aliquots, and the plates were incubated for 72 h. MTT (20 $\mu$L, 5 mg/mL Dulbecco's phosphate-buffered saline) was added to the cells, and the plates were incubated for a further 4 h. The culture medium was aspirated, and the purple formazan crystals formed by the mitochondrial dehydrogenase activity of vital cells were dissolved in DMSO (100 $\mu$L·well$^{-1}$). The absorbance of the resulting solutions, directly proportional to the number of surviving cells, was quantified at 590 nm using a SpectroMax M5e multimode microplate reader (using *SoftMax Pro* software, version 6.2.2). The percentage of surviving cells was calculated from the absorbance of wells corresponding to the untreated control cells. The reported IC50 values (Table 1) are based on the means from two independent experiments, each comprising four testings per concentration level.

## ■ ASSOCIATED CONTENT

### Supporting Information

The Supporting Information is available free of charge on the ACS Publications website at DOI: 10.1021/acs.inorgchem.8b00882.

Figures S1−S33 and Tables S1−S12, which include IR, NMR, and UV−vis spectra of compounds, solubility/stability studies in $H_2O$, chloride/solvent exchange experiments, cyclic voltammograms, and other information (PDF)

Cartesian coordinates of the DFT-optimized structures (XYZ)

### Accession Codes

CCDC 1816209 contains the supplementary crystallographic data for this paper. These data can be obtained free of charge via www.ccdc.cam.ac.uk/data_request/cif, or by emailing data_request@ccdc.cam.ac.uk, or by contacting The Cambridge Crystallographic Data Centre, 12 Union Road, Cambridge CB2 1EZ, UK; fax: +44 1223 336033.

## ■ AUTHOR INFORMATION


### Corresponding Author

*E-mail: fabio.marchetti1974@unipi.it. Webpage: https://people.unipi.it/fabio_marchetti1974/.

### ORCID

Stefano Zacchini: 0000-0003-0739-0518
Guido Pampaloni: 0000-0002-6375-4411
Paul J. Dyson: 0000-0003-3117-3249
Fabio Marchetti: 0000-0002-3683-8708


### Notes

The authors declare no competing financial interest.

## ■ ACKNOWLEDGMENTS

We thank the University of Pisa (PRA 2017: "Composti di metalli di transizione come possibili agenti antitumorali") and the Swiss National Science Foundation for financial support.



DOI: 10.1021/acs.inorgchem.8b00882
*Inorg. Chem.* XXXX, XXX, XXX−XXX

## REFERENCES


(1) Recent reviews on the topic include the following: (a) Johnstone, T. C.; Suntharalingam, K.; Lippard, S. J. *Chem. Rev.* **2016**, *116*, 3436−3486. (b) Zhang, P.; Sadler, P. J. *J. Organomet. Chem.* **2017**, *839*, 5−14. (c) Lazarevič, T.; Rilak, A.; Bugarčič, Z. D. *Eur. J. Med. Chem.* **2017**, *142*, 8−31. (d) Allardyce, C. S.; Dyson, P. J. *Dalton Trans.* **2016**, *45*, 3201−3209. (e) Barry, N. P. E.; Sadler, P. J. Exploration of the medical periodic table: towards new targets. *Chem. Commun.* **2013**, *49*, 5106−5041. (f) Bergamo, A.; Sava, G. *Chem. Soc. Rev.* **2015**, *44*, 8818−8835. (g) Zou, T.; Lum, C. T.; Lok, C.-N.; Zhang, J.-J.; Che, C.-M. *Chem. Soc. Rev.* **2015**, *44*, 8786−8801.

(2) Zeng, L.; Gupta, P.; Chen, Y.; Wang, E.; Ji, L.; Chao, H.; Chen, Z.-S. The development of anticancer ruthenium(II) complexes: from single molecule compounds to nanomaterials. *Chem. Soc. Rev.* **2017**, *46*, 5771−5804.

(3) (a) Alessio, E. Thirty Years of the Drug Candidate NAMI-A and the Myths in the Field of Ruthenium Anticancer Compounds: A Personal Perspective. *Eur. J. Inorg. Chem.* **2017**, *2017*, 1549−1560. and references cited therein (b) Trondl, R.; Heffeter, P.; Kowol, C. R.; Jakupec, M. A.; Berger, W.; Keppler, B. K. NKP-1339, the first ruthenium-based anticancer drug on the edge to clinical application. *Chem. Sci.* **2014**, *5*, 2925−2932. (c) Bytzek, A. K.; Koellensperger, G.; Keppler, B. K.; Hartinger, C. G. Biodistribution of the novel anticancer drug sodium trans-[tetrachloridobis(1H-indazole)ruthenate(III)] KP-1339/IT139 in nude BALB/c mice and implications on its mode of action. *J. Inorg. Biochem.* **2016**, *160*, 250−255. (d) Hartinger, C. G.; Jakupec, M. A.; Zorbas-Seifried, S.; Groessl, M.; Egger, A.; Berger, W.; Zorbas, H.; Dyson, P. J.; Keppler, B. K. KP1019, A New Redox-Active Anticancer Agent − Preclinical Development and Results of a Clinical Phase I Study in Tumor Patients. *Chem. Biodiversity* **2008**, *5*, 2140−2155. (e) Bergamo, A.; Sava, G. Ruthenium complexes can target determinants of tumour malignancy. *Dalton Trans.* **2007**, 1267−1272.

(4) (a) Bratsos, I.; Gianferrara, T.; Alessio, E.; Hartinger, C. G.; Jakupec, M. A.; Keppler, B. K. In *Bioinorganic Medicinal Chemistry*; Alessio, E., Ed.; Wiley-VCH: Weinheim, Germany, 2011; pp 151−174. (b) Clarke, M. J. Ruthenium metallopharmaceuticals. *Coord. Chem. Rev.* **2003**, *236*, 209−233. (c) Webb, M. I.; Chard, R. A.; Al-Jobory, Y. M.; Jones, M. R.; Wong, E. W. Y.; Walsby, C. J. Pyridine Analogues of the Antimetastatic Ru(III) Complex NAMI-A Targeting Non-Covalent Interactions with Albumin. *Inorg. Chem.* **2012**, *51*, 954−966.

(5) For instance, see: (a) Singh, A. K.; Pandey, D. S.; Xu, Q.; Braunstein, P. Recent advances in supramolecular and biological aspects of arene ruthenium(II) complexes. *Coord. Chem. Rev.* **2014**, *270*−*271*, 31−56. (b) Nazarov, A. A.; Hartinger, C. G.; Dyson, P. J. Opening the lid on piano-stool complexes: An account of ruthenium-(II)−arene complexes with medicinal applications. *J. Organomet. Chem.* **2014**, *751*, 251−260. (c) Basri, A. M.; Lord, R. M.; Allison, S. J.; Rodriguez-Barzano, A.; Lucas, S. J.; Janeway, F. D.; Shepherd, H. J.; Pask, C. M.; Phillips, R. M.; McGowan, P. C. Bis-picolinamide Ruthenium(III) Dihalide Complexes: Dichloride-to-Diiodide Exchange Generates Single trans Isomers with High Potency and Cancer Cell Selectivity. *Chem. - Eur. J.* **2017**, *23*, 6341−6356. (d) Meier, S. M.; Kreutz, D.; Winter, L.; Klose, M. H. M.; Cseh, K.; Weiss, T.; Bileck, A.; Alte, B.; Mader, J. C.; Jana, S.; Chatterjee, A.; Bhattacharyya, A.; Hejl, M.; Jakupec, M. A.; Heffeter, P.; Berger, W.; Hartinger, C. G.; Keppler, B. K.; Wiche, G.; Gerner, C. An Organoruthenium Anticancer Agent Shows Unexpected Target Selectivity For Plectin. *Angew. Chem., Int. Ed.* **2017**, *56*, 8267−8271. (e) Wang, Y.; Pitto-Barry, A.; Habtemariam, A.; Romero-Canelon, I.; Sadler, P. J.; Barry, N. P. E. Nanoparticles of chitosan conjugated to organo-ruthenium complexes. *Inorg. Chem. Front.* **2016**, *3*, 1058−1064.

(6) (a) Murray, B. S.; Babak, M. V.; Hartinger, C. G.; Dyson, P. J. The development of RAPTA compounds for the treatment of tumors. *Coord. Chem. Rev.* **2016**, *306*, 86−114. (b) Weiss, A.; Berndsen, R. H.; Dubois, M.; Müller, C.; Schibli, R.; Griffioen, A. W.; Dyson, P. J.; Nowak-Sliwinska, P. In vivo anti-tumor activity of the organometallic ruthenium(II)-arene complex [Ru($\eta^6$-p-cymene)$Cl_2$(pta)] (RAPTA-C) in human ovarian and colorectal carcinomas. *Chem. Sci.* **2014**, *5*, 4742−4748. (c) Murray, B. S.; Menin, L.; Scopelliti, R.; Dyson, P. J. Conformational control of anticancer activity: the application of arene-linked dinuclear ruthenium(II) organometallics. *Chem. Sci.* **2014**, *5*, 2536−2545. (d) Adhireksan, Z.; Davey, G. E.; Campomanes, P.; Groessl, M.; Clavel, C. M.; Yu, H.; Nazarov, A. A.; Yeo, C. H. F.; Ang, W. H.; Dröge, P.; Rothlisberger, U.; Dyson, P. J.; Davey, C. A. Ligand substitutions between ruthenium−cymene compounds can control protein versus DNA targeting and anticancer activity. *Nat. Commun.* **2014**, *5*, 1−13.

(7) (a) Morris, R. E.; Aird, R. E.; del Socorro Murdoch, P.; Chen, H.; Cummings, J.; Hughes, N. D.; Parsons, S.; Parkin, A.; Boyd, G.; Jodrell, D. I.; Sadler, P. J. Inhibition of Cancer Cell Growth by Ruthenium(II) Arene Complexes. *J. Med. Chem.* **2001**, *44*, 3616−3621. (b) Bergamo, A.; Masi, A.; Peacock, A. F. A.; Habtemariam, A.; Sadler, P. J.; Sava, G. In vivo tumour and metastasis reduction and in vitro effects on invasion assays of the ruthenium RM175 and osmium AFAP51 organometallics in the mammary cancer model. *J. Inorg. Biochem.* **2010**, *104*, 79−86. (c) Guichard, S. M.; Else, R.; Reid, E.; Zeitlin, B.; Aird, R.; Muir, M.; Dodds, M.; Fiebig, H.; Sadler, P. J.; Jodrell, D. I. Anti-tumour activity in non-small cell lung cancer models and toxicity profiles for novel ruthenium(II) based organo-metallic compounds. *Biochem. Pharmacol.* **2006**, *71*, 408−415. (d) Aird, R. E.; Cummings, J.; Ritchie, J.; Muir, M.; Morris, R. E.; Chen, H.; Sadler, P. J.; Jodrell, D. I. In vitro and in vivo activity and cross resistance profiles of novel ruthenium (II) organometallic arene complexes in human ovarian cancer. *Br. J. Cancer* **2002**, *86*, 1652−1657.

(8) (a) Habtemariam, A.; Melchart, M.; Fernandez, R.; Parsons, S.; Oswald, I. D. H.; Parkin, A.; Fabbiani, F. P. A.; Davidson, J. E.; Dawson, A.; Aird, R. E.; Jodrell, D. I.; Sadler, P. J. Structure−Activity Relationships for Cytotoxic Ruthenium(II) Arene Complexes Containing N,N-, N,O-, and O,O-Chelating Ligands. *J. Med. Chem.* **2006**, *49*, 6858−6868. (b) Soldevila-Barreda, J. J.; Romero-Canelon, I.; Habtemariam, A.; Sadler, P. J. Transfer hydrogenation catalysis in cells as a new approach to anticancer drug design. *Nat. Commun.* **2015**, *6*, 6582. (c) Bugarcic, T.; Habtemariam, A.; Stepankova, J.; Heringova, P.; Kasparkova, J.; Deeth, R. J.; Johnstone, R. D. L.; Prescimone, A.; Parkin, A.; Parsons, S.; Brabec, V.; Sadler, P. J. The Contrasting Chemistry and Cancer Cell Cytotoxicity of Bipyridine and Bipyridinediol Ruthenium(II) Arene Complexes. *Inorg. Chem.* **2008**, *47*, 11470−11486. (d) Delgado, R. A.; Galdamez, A.; Villena, J.; Reveco, P. G.; Thomet, F. A. Synthesis, characterization and in vitro biological evaluation of [Ru($\eta^6$-arene)(N,N)Cl]$PF_6$ compounds using the natural products arenes methylisoeugenol and anethole. *J. Organomet. Chem.* **2015**, *782*, 131−137. (e) Bugarcic, T.; Habtemariam, A.; Deeth, R. J.; Fabbiani, F. P. A.; Parsons, S.; Sadler, P. J. Ruthenium(II) Arene Anticancer Complexes with Redox-Active Diamine Ligands. *Inorg. Chem.* **2009**, *48*, 9444−9453.

(9) (a) Purkait, K.; Chatterjee, S.; Karmakar, S.; Mukherjee, A. Alteration of steric hindrance modulates glutathione resistance and cytotoxicity of three structurally related RuII-p-cymene complexes. *Dalton Trans.* **2016**, *45*, 8541−8555. (b) Wu, Q.; Zheng, K.; Liao, S.; Ding, Y.; Li, Y.; Mei, W. Arene Ruthenium(II) Complexes as Low-Toxicity Inhibitor against the Proliferation, Migration, and Invasion of MDA-MB-231 Cells through Binding and Stabilizing c-myc G-Quadruplex DNA. *Organometallics* **2016**, *35*, 317−326. (c) Sommer, M. G.; Kureljak, P.; Urankar, D.; Schweinfurth, D.; Stojanovic, N.; Bubrin, M.; Gazvoda, M.; Osmak, M.; Sarkar, B.; Košmrlj, J. Combining [Arene−Ru] with Azocarboxamide to Generate a Complex with Cytotoxic Properties. *Chem. - Eur. J.* **2014**, *20*, 17296−17299. (d) Miserachs, H. G.; Cipriani, M.; Grau, J.; Vilaseca, M.; Lorenzo, J.; Medeiros, A.; Comini, M. A.; Gambino, D.; Otero, L.; Moreno, V. Antitumor and antiparasitic activity of novel ruthenium compounds with polycyclic aromatic ligands. *J. Inorg. Biochem.* **2015**, *150*, 38−47. (e) Tian, M.; Li, J.; Zhang, S.; Guo, L.; He, X.; Kong, D.; Zhang, H.; Liu, Z. Half-sandwich ruthenium(II) complexes containing ÑN-chelated imino-pyridyl ligands that are selectively toxic to cancer cells. *Chem. Commun.* **2017**, *53*, 12810−12813.

(10) (a) Raghavan, A.; Venugopal, A. Review: Structurally characterized $\alpha$-diimine complexes of s- and p-block elements. *J. Coord. Chem.* **2014**, *67*, 2530−2549. (b) Guo, L.; Gao, H.; Guan, Q.;




DOI: 10.1021/acs.inorgchem.8b00882
*Inorg. Chem.* XXXX, XXX, XXX−XXX

Hu, H.; Deng, J.; Liu, J.; Liu, F.; Wu, Q. Substituent Effects of the Backbone in α-Diimine Palladium Catalysts on Homo- and Copolymerization of Ethylene with Methyl Acrylate. *Organometallics* **2012**, *31*, 6054−6062. (c) Uhlig, E. Non-innocent bidentate nitrogen-ligands in electron-rich complexes of 3d-elements. *Pure Appl. Chem.* **1988**, *60*, 1235−1240. (d) Van Koten, G.; Vrieze, K. 1,4-Diaza-1,3-butadiene (α-Diimine) Ligands: Their Coordination Modes and the Reactivity of Their Metal Complexes. *Adv. Organomet. Chem.* **1982**, *21*, 151−239.

(11) (a) Zuccaccia, D.; Bellachioma, G.; Cardaci, G.; Ciancaleoni, G.; Zuccaccia, C.; Clot, E.; Macchioni, A. Interionic Structure of Ion Pairs and Ion Quadruples of Half-Sandwich Ruthenium(II) Salts Bearing α-Diimine Ligands. *Organometallics* **2007**, *26*, 3930−3946. (b) Zuccaccia, D.; Sabatini, S.; Bellachioma, G.; Cardaci, G.; Clot, E.; Macchioni, A. PGSE and NOE NMR Evidence for Higher Order Aggregation in Some Cationic Ruthenium Complexes in Both Protic and Aprotic Solvents. *Inorg. Chem.* **2003**, *42*, 5465−5467. (c) Dieck, H. T.; Kollvitz, W.; Kleinwachter, I. Ruthenium complexes with diazadienes. 4. Arene diazadiene ruthenium(II) complexes $[(\eta^6\text{-arene})(RN{:}CR'{:}CR'{:}NR)Ru(L)]^{n+}$ (n = 1, L = Cl, I, alkyl; n = 2, L = MeCN, $\eta^2$-$C_2H_4$) and arene diazadiene ruthenium(0). *Organometallics* **1986**, *5*, 1449−1457.

(12) (a) Chari, R. V. J.; Miller, M. L.; Widdison, W. C. Antibody-drug conjugates: an emerging concept in cancer therapy. *Angew. Chem., Int. Ed.* **2014**, *53*, 3796−3827. (b) Hanif, M.; Meier, S. M.; Kandioller, W.; Bytzek, A.; Hejl, M.; Hartinger, C. G.; Nazarov, A. A.; Arion, V. B.; Jakupec, M. A.; Dyson, P. J.; Keppler, B. K. From hydrolytically labile to hydrolytically stable RuII−arene anticancer complexes with carbohydrate-derived co-ligands. *J. Inorg. Biochem.* **2011**, *105*, 224−231. (c) Margiotta, N.; Denora, N.; Ostuni, R.; Laquintana, V.; Anderson, A.; Johnson, S. W.; Trapani, G.; Natile, G. Platinum(II) Complexes with Bioactive Carrier Ligands Having High Affinity for the Translocator Protein. *J. Med. Chem.* **2010**, *53*, 5144−5154.

(13) For instance, see: (a) Kurzwernhart, A.; Kandioller, W.; Bächler, S.; Bartel, C.; Martic, S.; Buczkowska, M.; Mühlgassner, G.; Jakupec, M. A.; Kraatz, H.-B.; Bednarski, P. J.; Arion, V. B.; Marko, D.; Keppler, B. K.; Hartinger, C. G. Structure−Activity Relationships of Targeted RuII($\eta^6$-p-Cymene) Anticancer Complexes with Flavonol-Derived Ligands. *J. Med. Chem.* **2012**, *55*, 10512−10522. (b) Kandioller, W.; Balsano, E.; Meier, S. M.; Jungwirth, U.; Goschl, S.; Roller, A.; Jakupec, M. A.; Berger, W.; Keppler, B. K.; Hartinger, C. G. Organometallic anticancer complexes of lapachol: metal centre-dependent formation of reactive oxygen species and correlation with cytotoxicity. *Chem. Commun.* **2013**, *49*, 3348−3350. (c) Arion, V. B.; Dobrov, A.; Goschl, S.; Jakupec, M. A.; Keppler, B. K.; Rapta, P. Ruthenium- and osmium-arene-based paullones bearing a TEMPO free-radical unit as potential anticancer drugs. *Chem. Commun.* **2012**, *48*, 8559−8561. (d) Aman, F.; Hanif, M.; Kubanik, M.; Ashraf, A.; Söhnel, T.; Jamieson, S. M. F.; Siddiqui, W. A.; Hartinger, C. G. Anti-Inflammatory Oxicams as Multi-donor Ligand Systems: pH- and Solvent-Dependent Coordination Modes of Meloxicam and Piroxicam to Ru and Os. *Chem. - Eur. J.* **2017**, *23*, 4893−4902.

(14) (a) Nazarov, A. A.; Meier, S. M.; Zava, O.; Nosova, Y. N.; Milaeva, E. R.; Hartinger, C. G.; Dyson, P. J. Protein ruthenation and DNA alkylation: chlorambucil-functionalized RAPTA complexes and their anticancer activity. *Dalton Trans.* **2015**, *44*, 3614−3623. (b) Ang, W. H.; Parker, L. J.; De Luca, A.; Juillerat-Jeanneret, L.; Morton, C. J.; Lo Bello, M.; Parker, M. W.; Dyson, P. J. Rational design of an organometallic glutathione transferase inhibitor. *Angew. Chem., Int. Ed.* **2009**, *48*, 3854−3857.

(15) Selected recent references: (a) Păunescu, E.; Soudani, M.; Martin, P.; Scopelliti, R.; Lo Bello, M.; Dyson, P. J. Organometallic Glutathione S-Transferase Inhibitors. *Organometallics* **2017**, *36*, 3313−3321. (b) Ashraf, A.; Hanif, M.; Kubanik, M.; Söhnel, T.; Jamieson, S. M. F.; Bhattacharyya, A.; Hartinger, C. G. Aspirin-inspired organometallic compounds: Structural characterization and cytotoxicity. *J. Organomet. Chem.* **2017**, *839*, 31−37. (c) Biancalana, L.; Batchelor, L. K.; De Palo, A.; Zacchini, S.; Pampaloni, G.; Dyson, P. J.; Marchetti, F. *A general strategy to add diversity to ruthenium arene complexes with bioactive organic compounds via a coordinated (4-hydroxyphenyl) diphenylphosphine ligand Dalton Trans.* **2017**, *46*, 12001−12004. (d) Babak, M. V.; Plazuk, D.; Meier, S. M.; Arabshahi, H. J.; Reynisson, J.; Rychlik, B.; Błauz, A.; Szulc, K.; Hanif, M.; Strobl, S.; Roller, A.; Keppler, B. K.; Hartinger, C. G. Half-Sandwich Ruthenium-(II) Biotin Conjugates as Biological Vectors to Cancer Cells. *Chem. - Eur. J.* **2015**, *21*, 5110−5117. (e) Biancalana, L.; Pratesi, A.; Chiellini, F.; Zacchini, S.; Funaioli, T.; Gabbiani, C.; Marchetti, F. Ruthenium arene complexes with triphenylphosphane ligands: cytotoxicity towards pancreatic cancer cells, interaction with model proteins, and effect of ethacrynic acid substitution. *New J. Chem.* **2017**, *41*, 14574−14588.

(16) Kliegman, J. M.; Barnes, R. K. Glyoxal derivatives-I: Conjugated aliphatic diimines from glyoxal and aliphatic primary amines. *Tetrahedron* **1970**, *26*, 2555−2560.

(17) Kliegman, J. M.; Barnes, R. K. Glyoxal derivatives. II. Reaction of glyoxal with aromatic primary amines. *J. Org. Chem.* **1970**, *35*, 3140−3143.

(18) Dieck, H. T.; Renk, I. W. Kupfer(I)-diazabutadien-halogenide. *Chem. Ber.* **1971**, *104*, 92−109.

(19) Selected recent references: (a) Palmucci, J.; Marchetti, F.; Pettinari, R.; Pettinari, C.; Scopelliti, R.; Riedel, T.; Therrien, B.; Galindo, A.; Dyson, P. J. Synthesis, Structure, and Anticancer Activity of Arene−Ruthenium(II) Complexes with Acylpyrazolones Bearing Aliphatic Groups in the Acyl Moiety. *Inorg. Chem.* **2016**, *55*, 11770−11781. (b) Kubanik, M.; Holtkamp, H.; Söhnel, T.; Jamieson, S. M. F.; Hartinger, C. G. Impact of the Halogen Substitution Pattern on the Biological Activity of Organoruthenium 8-Hydroxyquinoline Anticancer Agents. *Organometallics* **2015**, *34*, 5658−5668. (c) Clavel, C. M.; Păunescu, E.; Nowak-Sliwinska, P.; Griffioen, A. W.; Scopelliti, R.; Dyson, P. J. Modulating the Anticancer Activity of Ruthenium(II)−Arene Complexes. *J. Med. Chem.* **2015**, *58*, 3356−3365. (d) Hackenberg, F.; Müller-Bunz, H.; Smith, R.; Streciwilk, W.; Zhu, X.; Tacke, M. Novel Ruthenium(II) and Gold(I) NHC Complexes: Synthesis, Characterization, and Evaluation of Their Anticancer Properties. *Organometallics* **2013**, *32*, 5551−5560. (e) Grgurić-Šipka, S.; Ivanović, I.; Rakić, G.; Todorović, N.; Gligorijević, N.; Radulović, S.; Arion, V. B.; Keppler, B. K.; Tešic, Z. L. Ruthenium(II)−arene complexes with functionalized pyridines: Synthesis, characterization and cytotoxic activity. *Eur. J. Med. Chem.* **2010**, *45*, 1051−1058.

(20) Menon, M.; Pramanik, A.; Chakravorty, A. Amide Formation from Aldimine and Water Promoted by Coordinated Metal Redox. Chemistry of a Family of Isomeric RuII(diimine)$_2$Cl$_2$, RuIII-(diimine)$_2$Cl$_2^+$, and RuIII(diimine)(amide-imine)Cl$_2$ Complexes. *Inorg. Chem.* **1995**, *34*, 3310−3316.

(21) Attempted esterification protocols: (1) RCOCl/Et$_3$N; (2) RCO$_2$H/EDCI·HCl/DMAP (Steglich esterification); (3) RCO$_2$H/BOP-Cl/Et$_3$N [BOP-Cl = bis(2-oxo-3-oxazolidinyl)phosphinic chloride].

(22) Morrone, S.; Guillon, D.; Bruce, D. W. Synthesis and Structures of Intramolecularly Base-Coordinated Aryl Group 15 Compounds. *Inorg. Chem.* **1996**, *35*, 7041−7048.

(23) Chan, S. H.; Lam, L. S. M.; Tse, C. W.; Man, K. Y. K.; Wong, W. T.; Djurišić, A. B.; Chan, W. K. Photosensitivity of Functional Polystyrene and Poly(methyl methacrylate) Synthesized by Controlled Radical Polymerization. *Macromolecules* **2003**, *36*, 5482−5490.

(24) For aspirin, some selected references are as follows: (a) Yiannakopoulou, E. Ch. Aspirin and NSAIDs for breast cancer chemoprevention. *Eur. J. Cancer Prev.* **2015**, *24*, 416−421. (b) Rothwell, P. M.; Fowkes, F. G. R.; Belch, J. F. F.; Ogawa, H.; Warlow, C. P.; Meade, T. W. Effect of daily aspirin on long-term risk of death due to cancer: analysis of individual patient data from randomised trials. *Lancet* **2011**, *377*, 31−41. (c) Din, F. V. N.; Valanciute, A.; Houde, V. P.; Zibrova, D.; Green, K. A.; Sakamoto, K.; Alessi, D. R.; Dunlop, M. G. Aspirin inhibits mTOR signaling, activates AMP-activated protein kinase, and induces autophagy in colorectal cancer cells. *Gastroenterology* **2012**, *142*, 1504−1515.

(25) For valproic acid, some selected references are as follows: (a) Caponigro, F.; Di Gennaro, E.; Ionna, F.; Longo, F.; Aversa, C.;



DOI: 10.1021/acs.inorgchem.8b00882
*Inorg. Chem.* XXXX, XXX, XXX−XXX

Pavone, E.; Maglione, M. G.; Di Marzo, M.; Muto, P.; Cavalcanti, E.; Petrillo, A.; Sandomenico, F.; Maiolino, P.; D'Aniello, R.; Botti, G.; De Cecio, R.; Losito, N. S.; Scala, S.; Trotta, A.; Zotti, A. I.; Bruzzese, F.; Daponte, A.; Calogero, E.; Montano, M.; Pontone, M.; De Feo, G.; Perri, F.; Budillon, F. Phase II clinical study of valproic acid plus cisplatin and cetuximab in recurrent and/or metastatic squamous cell carcinoma of Head and Neck-V-CHANCE trial. *BMC Cancer* **2016**, *16*, 918. (b) Groh, T.; Hrabeta, J.; Khalil, M. A.; Doktorova, H.; Eckschlager, T.; Stiborova, M. The synergistic effects of DNA-damaging drugs cisplatin and etoposide with a histone deacetylase inhibitor valproate in high-risk neuroblastoma cells. *Int. J. Oncol.* **2015**, *47*, 343−352. (c) Rocca, A.; Minucci, S.; Tosti, G.; Croci, D.; Contegno, F.; Ballarini, M.; Nolè, F.; Munzone, E.; Salmaggi, A.; Goldhirsch, A.; Pelicci, P. G.; Testori, A. A phase I−II study of the histone deacetylase inhibitor valproic acid plus chemoimmunotherapy in patients with advanced melanoma. *Br. J. Cancer* **2009**, *100*, 28−36.

(26) Aspirin: (a) Rubner, G.; Bensdorf, K.; Wellner, A.; Kircher, B.; Bergemann, S.; Ott, I.; Gust, R. Synthesis and Biological Activities of Transition Metal Complexes Based on Acetylsalicylic Acid as Neo-Anticancer Agents. *J. Med. Chem.* **2010**, *53*, 6889−6898. (b) Cheng, Q.; Shi, H.; Wang, H.; Min, Y.; Wang, J.; Liu, Y. The ligation of aspirin to cisplatin demonstrates significant synergistic effects on tumor cells. *Chem. Commun.* **2014**, *50*, 7427−7430.

(27) Valproic acid: (a) Raveendran, R.; Braude, J. P.; Wexselblatt, E.; Novohradsky, V.; Stuchlikova, O.; Brabec, V.; Gandin, V.; Gibson, D. Pt(IV) derivatives of cisplatin and oxaliplatin with phenylbutyrate axial ligands are potent cytotoxic agents that act by several mechanisms of action. *Chem. Sci.* **2016**, *7*, 2381−2391. (b) Ravera, M.; Gabano, E.; Zanellato, I.; Gallina, A.; Perin, E.; Arrais, A.; Cantamessa, S.; Osella, D. Cisplatin and valproate released from the bifunctional [Pt(IV)-$Cl_2(NH_3)_2(valproato)_2$] antitumor prodrug or from liposome formulations: who does what? *Dalton Trans.* **2017**, *46*, 1559−1566.

(28) Neises, B.; Steglich, W. Simple Method for the Esterification of Carboxylic Acids. *Angew. Chem., Int. Ed. Engl.* **1978**, *17*, 522−524.

(29) (a) Păunescu, E.; Soudani, M.; Clavel, C. M.; Dyson, P. J. Varying the metal to ethacrynic acid ratio in ruthenium(ii)/osmium(ii)-p-cymene conjugates. *J. Inorg. Biochem.* **2017**, *175*, 198−207. (b) Păunescu, E.; McArthur, S.; Soudani, M.; Scopelliti, R.; Dyson, P. J. Nonsteroidal Anti-inflammatory—Organometallic Anticancer Compounds. *Inorg. Chem.* **2016**, *55*, 1788−1808.

(30) Despite being well soluble in $CDCl_3$, NMR characterization of [**4**−**6**]X (X = Cl and $NO_3$) could not be performed in this solvent because of broadening of the $^1$H resonances.

(31) Herbison-Evans, D.; Richards, R. E. $^{14}$N chemical shifts in organic compounds. *Mol. Phys.* **1964**, *8*, 19−31.

(32) Rundlöf, T.; Mathiasson, M.; Bekiroglu, S.; Hakkarainen, B.; Bowden, T.; Arvidsson, T. Survey and qualification of internal standards for quantification by $^1$H NMR spectroscopy. *J. Pharm. Biomed. Anal.* **2010**, *52*, 645−651.

(33) Wu, Y. C.; Berezansky, P. A. Low Electrolytic Conductivity Standards. *J. Res. Natl. Inst. Stand. Technol.* **1995**, *100*, 521−527.

(34) $^{35}$Cl NMR spectra of [**1**−**3**]$NO_3$/1:9 $D_2O/CD_3OD$ solutions ($c_{Ru} = 10^{-2}$ M) showed no signal compared with an equimolar NaCl solution in the same solvent, giving an intense sharp resonance ($\delta_{Cl}$ = 3 ppm) in less than one-third of the acquisition time.

(35) Coordinated $H_2O$ is expected to be quite acidic in a dicationic complex. For comparison, a p$K_a$ value of 8.24 was determined for structurally related [(*p*-cymene)Ru($H_2O$)(en)]$^{2+}$. Chen, H.; Parkinson, J. A.; Morris, R. E.; Sadler, P. J. Highly Selective Binding of Organometallic Ruthenium Ethylenediamine Complexes to Nucleic Acids: Novel Recognition Mechanisms. *J. Am. Chem. Soc.* **2003**, *125*, 173−186.

(36) Scolaro, C.; Bergamo, A.; Brescacin, L.; Delfino, R.; Cocchietto, M.; Laurenczy, G.; Geldbach, T. J.; Sava, G.; Dyson, P. J. In Vitro and in Vivo Evaluation of Ruthenium(II)−Arene PTA Complexes. *J. Med. Chem.* **2005**, *48*, 4161−4171.

(37) Wang, F.; Chen, H.; Parsons, S.; Oswald, I. D. H.; Davidson, J. E.; Sadler, P. J. Kinetics of Aquation and Anation of Ruthenium(II) Arene Anticancer Complexes, Acidity and X-ray Structures of Aqua Adducts. *Chem. - Eur. J.* **2003**, *9*, 5810−5820.

(38) All potentials are referred to NHE.

(39) Gras, M.; Therrien, B.; Süss-Fink, G.; Štepnicka, P.; Renfrew, A. K.; Dyson, P. J. Water-soluble arene ruthenium complexes containing pyridinethiolato ligands: Synthesis, molecular structure, redox properties and anticancer activity of the cations [($\eta^6$-arene)Ru(p-$SC_5H_4NH)_3$]$^{2+}$. *J. Organomet. Chem.* **2008**, *693*, 3419−3424.

(40) (a) Wang, X.; Zhao, Y.; Gong, S.; Liu, B.; Li, Q. S.; Su, J. H.; Wu, B.; Yang, X. J. Mono- and Dinuclear Heteroleptic Cobalt Complexes with $\alpha$-Diimine and Polyarene Ligands. *Chem. - Eur. J.* **2015**, *21*, 13302−13310. (b) Cole, B. E.; Wolbach, J. P.; Dougherty, W. J., Jr.; Piro, N. A.; Kassel, W. S.; Graves, C. R. Synthesis and Characterization of Aluminum-$\alpha$-diimine Complexes over Multiple Redox State. *Inorg. Chem.* **2014**, *53*, 3899−3906. (c) Li, J.; Zhang, K.; Huang, H.; Yu, A.; Hu, H.; Cui, H.; Cui, C. Synthesis and Reactions of a Redox-Active $\alpha$-Diimine Aluminum Complex. *Organometallics* **2013**, *32*, 1630−1635. (d) Mealli, C.; Ienco, A.; Phillips, A. D.; Galindo, A. A Critical Review of Electronic Effects in Enediamido and $\alpha$-Diimino Complexes of the Group 4 Metals. *Eur. J. Inorg. Chem.* **2007**, *2007*, 2556−2568. (e) Daff, P. J.; Etienne, M.; Donnadieu, B.; Knottenbelt, S. Z.; McGrady, J. E. Stable Formally Zerovalent and Diamagnetic Monovalent Niobium and Tantalum Complexes Based on Diazadiene Ligands. *J. Am. Chem. Soc.* **2002**, *124*, 3818−3819.

(41) Zanello, P. *Inorganic Electrochemistry: Theory, Practice and Application*; The Royal Society of Chemistry, 2003.

(42) Kirlin, W. G.; Cai, J.; Thompson, S. A.; Diaz, D.; Kavanagh, T. J.; Jones, D. P. Glutathione redox potential in response to differentiation and enzyme inducers. *Free Radical Biol. Med.* **1999**, *27*, 1208−1218.

(43) (a) Griffith, D. M.; Duff, B.; Suponitsky, K. Y.; Kavanagh, K.; Morgan, M. P.; Egan, D.; Marmion, C. J. Novel trans-platinum complexes of the histone deacetylase inhibitor valproic acid; synthesis, in vitro cytotoxicity and mutagenicity. *J. Inorg. Biochem.* **2011**, *105*, 793−799. (b) Novohradsky, V.; Zerzankova, L.; Stepankova, J.; Vrana, O.; Raveendran, R.; Gibson, D.; Kasparkova, J.; Brabec, V. New insights into the molecular and epigenetic effects of antitumor Pt(IV)-valproic acid conjugates in human ovarian cancer cells. *Biochem. Pharmacol.* **2015**, *95*, 133−144.

(44) Bennett, M. A.; Smith, A. K. Arene ruthenium(II) complexes formed by dehydrogenation of cyclohexadienes with ruthenium(III) trichloride. *J. Chem. Soc., Dalton Trans.* **1974**, 233−241.

(45) Gottlieb, H. E.; Kotlyar, V.; Nudelman, A. NMR Chemical Shifts of Common Laboratory Solvents as Trace Impurities. *J. Org. Chem.* **1997**, *62*, 7512−7515.

(46) Harris, R. K.; Becker, E. D.; Cabral de Menezes, S. M.; Goodfellow, R.; Granger, P. NMR nomenclature. Nuclear spin properties and conventions for chemical shifts (IUPAC Recommendations 2001). *Pure Appl. Chem.* **2001**, *73*, 1795−1818.

(47) Willker, W.; Leibfritz, D.; Kerssebaum, R.; Bermel, W. Gradient selection in inverse heteronuclear correlation spectroscopy. *Magn. Reson. Chem.* **1993**, *31*, 287−292.

(48) Menges, F. *Spectragryph: optical spectroscopy software*, version 1.2.5; 2016−2017; http://www.effemm2.de/spectragryph.

(49) (a) Jutand, A. The Use of Conductivity Measurements for the Characterization of Cationic Palladium(II) Complexes and for the Determination of Kinetic and Thermodynamic Data in Palladium-Catalyzed Reactions. *Eur. J. Inorg. Chem.* **2003**, *2003*, 2017−2040. (b) Geary, W. J. The use of conductivity measurements in organic solvents for the characterisation of coordination compounds. *Coord. Chem. Rev.* **1971**, *7*, 81−122.

(50) Sheldrick, G. M. *SADABS-2008/1: Bruker AXS Area Detector Scaling and Absorption Correction*; Bruker AXS: Madison, WI, 2008.

(51) Sheldrick, G. M. Crystal structure refinement with SHELXL. *Acta Crystallogr., Sect. C: Struct. Chem.* **2015**, *71*, 3−8.

(52) With the exception of the most acidic (pH = 1.57) and basic (pH = 12.2) solutions, which were not included in the calculation of p$K_a$, the main contribution to the ionic strength (*I*) is given by NaCl (0.1 M).



DOI: 10.1021/acs.inorgchem.8b00882
*Inorg. Chem.* XXXX, XXX, XXX−XXX

(53) (a) Westcott, C. C. *pH Measurements*; Academic Press: New York, 1978. (d) Covington, A. K.; Paabo, M.; Robinson, R. A.; Bates, R. G. Use of the glass electrode in deuterium oxide and the relation between the standardized pD (paD) scale and the operational pH in heavy water. *Anal. Chem.* **1968**, *40*, 700−706.
(54) The solubility of $[3]NO_3$ in water ($5.6 \times 10^{-3}$ M) jointly with the relatively high value of $pK_a$ for $[3]^+$ (7.7) prevented its determination via potentiometric NaOH titration (the pH vs added base curve showed no appreciable inflection).
(55) (a) Albert, A.; Serjeant, E. P. *The Determination of Ionization Constants*; Chapman & Hall: London, 1984; pp 70−75. (b) Salgado, L. E. V.; Vargas-Hernández, C. Spectrophotometric Determination of the pKa, Isosbestic Point and Equation of Absorbance vs. pH for a Universal pH Indicator. *Am. J. Anal. Chem.* **2014**, *5*, 1290−1301.
(56) Rice, N. M.; Irving, H. M. N. H.; Leonard, M. A. Nomenclature for liquid-liquid distribution (solvent extraction) (IUPAC Recommendations **1993**). *Pure Appl. Chem.* **1993**, *65*, 2373−2396.
(57) *OECD Guidelines for Testing of Chemicals*; OECD, Paris, 1995; Vol. *107*.
(58) (a) Minenkov, Y.; Singstad, A.; Occhipinti, G.; Jensen, V. R. The accuracy of DFT-optimized geometries of functional transition metal compounds: a validation study of catalysts for olefin metathesis and other reactions in the homogeneous phase. *Dalton Trans.* **2012**, *41*, 5526−5541. (b) Chai, J.-D.; Head-Gordon, M. Long-range corrected hybrid density functionals with damped atom−atom dispersion corrections. *Phys. Chem. Chem. Phys.* **2008**, *10*, 6615−6620. (c) Gerber, I. C.; Ángyán, J. G. Hybrid functional with separated range. *Chem. Phys. Lett.* **2005**, *415*, 100−105.
(59) (a) Weigend, F.; Ahlrichs, R. Balanced basis sets of split valence, triple zeta valence and quadruple zeta valence quality for H to Rn: Design and assessment of accuracy. *Phys. Chem. Chem. Phys.* **2005**, *7*, 3297−3305. (b) Andrae, D.; Häußermann, U.; Dolg, M.; Stoll, H.; Preuß, H. Energy-adjusted ab initio pseudopotentials for the second and third row transition elements. *Theor. Chim. Acta* **1990**, *77*, 123−141.
(60) (a) Cossi, M.; Rega, N.; Scalmani, G.; Barone, V. Energies, structures, and electronic properties of molecules in solution with the C-PCM solvation model. *J. Comput. Chem.* **2003**, *24*, 669−681. (b) Barone, V.; Cossi, M. Quantum Calculation of Molecular Energies and Energy Gradients in Solution by a Conductor Solvent Model. *J. Phys. Chem. A* **1998**, *102*, 1995−2001.
(61) Jensen, F. *Introduction to Computational Chemistry*, 2nd ed.; Wiley: Chichester, U.K., 2007.
(62) Frisch, M. J.; Trucks, G. W.; Schlegel, H. B.; Scuseria, G. E.; Robb, M. A.; Cheeseman, J. R.; Scalmani, G.; Barone, V.; Mennucci, B.; Petersson, G. A.; Nakatsuji, H.; Caricato, M.; Li, X.; Hratchian, H. P.; Izmaylov, A. F.; Bloino, J.; Zheng, G.; Sonnenberg, J. L.; Hada, M.; Ehara, M.; Toyota, K.; Fukuda, R.; Hasegawa, J.; Ishida, M.; Nakajima, T.; Honda, Y.; Kitao, O.; Nakai, H.; Vreven, T.; Montgomery, J. A., Jr.; Peralta, J. E.; Ogliaro, F.; Bearpark, M.; Heyd, J. J.; Brothers, E.; Kudin, K. N.; Staroverov, V. N.; Kobayashi, R.; Normand, J.; Raghavachari, K.; Rendell, A.; Burant, J. C.; Iyengar, S. S.; Tomasi, J.; Cossi, M.; Rega, N.; Millam, J. M.; Klene, M.; Knox, J. E.; Cross, J. B.; Bakken, V.; Adamo, C.; Jaramillo, J.; Gomperts, R.; Stratmann, R. E.; Yazyev, O.; Austin, A. J.; Cammi, R.; Pomelli, C.; Ochterski, J. W.; Martin, R. L.; Morokuma, K.; Zakrzewski, V. G.; Voth, G. A.; Salvador, P.; Dannenberg, J. J.; Dapprich, S.; Daniels, A. D.; Farkas, Ö.; Foresman, J. B.; Ortiz, J. V.; Cioslowski, J.; Fox, D. J. *Gaussian 09*, revision C.01; Gaussian, Inc.: Wallingford, CT, 2009.
(63) A value of $E_{ref}$ = +0.205 V versus NHE was obtained, in agreement with the literature data for similar Ag/AgCl/KCl electrodes. *Electrochemistry for Chemists*, 2nd ed.; Sawyer, D. T., Sobkowiak, A. J., Roberts, J., Jr., Eds.; John Wiley & Sons: New York, 1995; section 5.2.
(64) Gross, M.; Jordan, J. Voltammetry At Glassy Carbon Electrodes. *Pure Appl. Chem.* **1984**, *56*, 1095−1129.
(65) Reference value for the $Fe(CN)_6^{3-}/Fe(CN)_6^{4-}$ couple: $E_{1/2}$ = +0.256 V versus 4 M Ag/AgCl/KCl in a 0.1 M phosphate buffer solution (pH = 7.4) + 1 M KCl (given in ref 64).
(66) Bonuccelli, V.; Funaioli, T.; Leoni, P.; Marchetti, F.; Marchetti, L.; Pasquali, M. Synthesis and characterization of non-bridging mono- and bis-$\sigma$-$\eta^1$-alkynyl derivatives of the phosphido-bridged hexaplatinum core $[Pt_6(\mu\text{-}PBut_2)_4(CO)_4]^{2+}$. *Dalton Trans* **2016**, *45*, 6878−6892.
(67) Mosmann, T. Rapid colorimetric assay for cellular growth and survival: application to proliferation and cytotoxicity assays. *J. Immunol. Methods* **1983**, *65*, 55−63.


DOI: 10.1021/acs.inorgchem.8b00882
*Inorg. Chem.* XXXX, XXX, XXX−XXX